



저작자표시-비영리-변경금지 2.0 대한민국

이용자는 아래의 조건을 따르는 경우에 한하여 자유롭게

- 이 저작물을 복제, 배포, 전송, 전시, 공연 및 방송할 수 있습니다.

다음과 같은 조건을 따라야 합니다:



저작자표시. 귀하는 원저작자를 표시하여야 합니다.



비영리. 귀하는 이 저작물을 영리 목적으로 이용할 수 없습니다.



변경금지. 귀하는 이 저작물을 개작, 변형 또는 가공할 수 없습니다.

- 귀하는, 이 저작물의 재이용이나 배포의 경우, 이 저작물에 적용된 이용허락조건을 명확하게 나타내어야 합니다.
- 저작권자로부터 별도의 허가를 받으면 이러한 조건들은 적용되지 않습니다.

저작권법에 따른 이용자의 권리는 위의 내용에 의하여 영향을 받지 않습니다.

이것은 [이용허락규약\(Legal Code\)](#)을 이해하기 쉽게 요약한 것입니다.

[Disclaimer](#)

Thesis for the Degree of Master of Engineering

Numerical Study on the Evaluation of Lubrication Performance of Journal Bearing

by

Kyeong Hwan Kim

Mechanical Design Engineering

The Graduate School

Pukyong National University

August, 2020

수치해석에 의한 저널 베어링 윤활 성능평가

Advisor: Prof. Yeon Won Lee

by
Kyeong Hwan Kim

A thesis submitted in partial fulfillment of the requirements
for the degree of

Master of Engineering

Mechanical Design Engineering,
The Graduate School,
Pukyong National University

August 2020

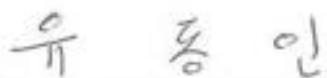
Numerical Study on the Evaluation of Lubrication
Performance of Journal Bearing

A dissertation
by
Kyeong Hwan Kim

Approved by:



Prof. Kyoung Joon Kim (Chairman)



Prof. Dong In Yu (Member)



Prof. Yeon Won Lee (Member)

August, 2020

Numerical Study on the Evaluation of Lubrication Performance of Journal Bearing

Kyeong Hwan Kim

Mechanical Design Engineering,
The Graduate School,
Pukyong National University

Abstract

A bearing is a mechanical element that supports shaft loads and assists in rotating the machine that cannot be excluded while discussing mechanical devices. Among them, journal bearings are used for high loads or high speed rotating motions due to their large area under loads and small friction coefficients. In the lubrication analysis of bearings, it is common to use Reynolds equation, which takes into account the low Reynolds number that can ignore the inertial terms compared to the viscous terms. However, as the eccentricity increases with higher loads and higher speeds, the flow becomes more complex, and for flows with high Reynolds number, it is necessary to simultaneously introduce the turbulence model and Navier-Stokes equation to calculate the viscosity flow.

In this study, we analyze various factors affecting the bearing lubrication such as the lubrication temperature (50 °C , 100 °C , 150 °C , 180 °C , 200 °C), the shape of the bearing (considering the dimple structure), the rotational speed (1000 RPM, 2000 RPM, 3000 RPM, 4000 RPM, 5000 RPM), and the eccentricity (0.6, 0.8 and 0.9). The elements that can determine bearing performance – such as pressure distribution of bearing parts, attitude angle according to the load on the shaft and volume fraction of lubricants in the gas state – were checked and compared according to Korea Standard (KS). The results showed that when the eccentricity and the rotational speed is increased and the lubricant temperature is lowered, the pressure on the bearings are increased. The results also matched well with the experimental results. By introducing the dimple structure on the bearing, the performance is improved when compared to that of the plain bearing. The dimple structure reduces the

contact area between the shaft and the bearing, and the volume fraction reduction prevents erosion inside the bearing due to cavitation.



수치해석에 의한 저널 베어링 윤활 성능평가

김경환

기계설계공학과
대학원,
부경대학교

초록

축의하중을 지지하고 기계의 회전운동을 돕는 베어링은 기계장치를 논할 때 배제할 수 없는 요소이다. 그 중에서도 저널 베어링은 하중을 받는 면적이 넓고 마찰 계수가 작아 높은 하중이나 고속으로 회전하는 운동을 필요로 할 때 사용된다. 베어링의 윤활 해석에서는 점성항과 비교하여 관성항을 무시할 수 있는 낮은 레이놀즈수를 고려한 Reynolds equation을 사용하는 것이 일반적이다. 하지만 고하중과 고속으로 갈수록 편심도는 높아지고 흐름은 복잡해지며 높은 레이놀즈 수를 가진 유동으로 천이함에 따라 난류 모델과 Navier-Stokes 방정식을 동시에 도입하여 점성유동을 계산할 필요가 있다. 베어링 윤활에 영향을 주는 여러 가지 인자 중 본 연구에서는 윤활 온도(50°C, 100°C, 150°C, 180°C, 200°C), 베어링의 형상(Dimple 구조물을 고려), 회전 속도(1000RPM, 2000RPM, 3000RPM, 4000RPM, 5000RPM) 그리고 편심도(0.6, 0.8, 0.9)를 고려하여 해석하였다. 해석된 결과를 바탕으로 베어링부의 압력분포, 축에 걸리는 하중에 따른 자세각 그리고 기체 상태의 윤활제 부피비 등 베어링 성능을 판단할 수 있는 요소를 확인하고 KS 규격에 따라 비교 분석을 하였다. 그 결과는 온도가 낮아지고, 편심도가 커지고 회전 속도가 높아짐에 따라서 베어링에 가해지는 압력도 커짐을 알 수 있었고, 실험 결과와 잘 일치함을 확인하였다. 또한 수치해석 결과로부터 덤플

구조물을 삽입함으로써 베어링의 성능을 향상시킬 수 있었고, 댐플 구조물에 윤활제가 채워지게 되어 경계 윤활 및 고체 윤활을 완화할 수 있었다.



Acknowledgement

It was during my bachelors second year (November 2016) that I came to know about Professor Yeon Won Lee by word of mouth in one of my classes. One fine day, without a prior appointment, I went to meet him in his office. He greeted me warmly and I consulted with him for a long time regarding a lab to study. I was surprised to see Professor Yeon Won Lee gave full attention to my consultation irrespective of not knowing me and introduced me to his lab (CFD and Energy Systems Laboratory) members and offered a chance to study under him the same day. Since then, I have been connected with the lab. During my time in the lab, there were hard times in personal relationships and academics, but it seemed to be a valuable time that I had acquired a wealth of academic experiences with good colleagues and seniors. And these times would not have existed if Professor Yeon Won Lee hadn't been there.

I want to appreciate and say thank you to my beloved father, the head of the family, who supports me in whatever I want to do, keeps a close eye on me, and tells me the right thing every time whenever I'm struggling at the crossroads. Beloved mother, I want you to know that I have grown up now and I am on the right track in pursuit of a good future. Even though I have fought a lot, I would like to say thank you to my elder sister who was always on my side as a friend when I was young, as a mentor in school and as a strong supporter even after becoming an adult.

I would like to thank my lab members Jeon Junho, Hongwu Zhao, Palash Chakma, Dr. Parthasarathy Nanjundan (Parth), and Dr. Yoon Hwan Choi. Mr. Jeon Junho, who was the most reliable and dependable supporter and senior in the lab; Mr. Hongwu Zhao and Mr. Palash Chakma, two trusted friends, who helped a lot and took care of me at difficult times; Mr. Parth, sometimes like a friend, sometimes as a teacher, who gave a lot of advice in life and research; Also, I would like to thank Dr. Yoon-Hwan Choi for giving a lot of practical advice, and Professor Dong-In Yu, who is always friendly. Also, I would like to thank all my professors of the Department of Mechanical Design Engineering, Pukyong National University, Busan, South Korea.

Lastly, I would like to tell about myself that I believe in me and have no doubts about my ability and my way, and that I will focus and move forward towards my future and I ask you to take care of your future as well. Thank you.

July 22, 2020.

Busan, South Korea.

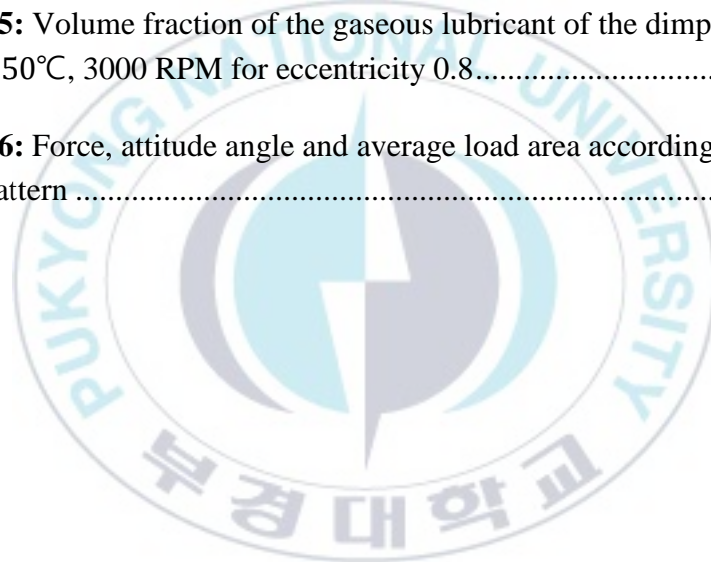
List of Figures

Figure 2.1: CFD interpretation process.....	9
Figure 2.2: Shear force between two planes	18
Figure 2.3: Pressure distribution during bearing operation	20
Figure 2.4: Bearing nomenclature	21
Figure 2.5: Flowchart of bearing characteristic calculation	26
Figure 3.1: Bearing boundary conditions used in numerical analysis	33
Figure 3.2: Modeling process of journal bearing flow field. (a) journal bearing; (b) flow field of journal bearing; (c) flow field model used for analysis.....	34
Figure 3.3: Analysis result according to the number of mesh of lubrication thickness.....	36
Figure 3.4: Analysis result according to the number of mesh of bearing width direction	37
Figure 3.5: Analysis result according to the number of mesh of circumferential direction	38
Figure 3.6: Comparison of experimental and numerical analysis results according to the rotational speed of the shaft	39
Figure 3.7: Comparison of experimental and numerical analysis results according to the eccentricity	40

Figure 3.8: Viscosity change of lubricant (TP-30) with temperature by Andrade Equation	42
Figure 3.9: Variation of saturated vapor pressure with temperature	43
Figure 3.10: Pressure field according to temperature change at 3000RPM for eccentricity is 0.6	45
Figure 3.11: Pressure field according to temperature change at 3000RPM for eccentricity is 0.8	46
Figure 3.12: Pressure field according to temperature change at 3000RPM for eccentricity is 0.9	47
Figure 3.13: Plane view projection in the circumferential direction of the bearing.....	48
Figure 3.14: Circumferential pressure data applied to the bearing part.....	48
Figure 3.15: Plane view projection in the width direction of the bearing	50
Figure 3.16: Volume fraction of the gaseous lubricant in the width direction of the bearing according to the temperature at 3000RPM when the eccentricity is 0.6.....	50
Figure 3.17: Volume fraction of the gaseous lubricant in the width direction of the bearing according to the temperature at 3000RPM when the eccentricity is 0.8.....	51
Figure 3.18: Volume fraction of the gaseous lubricant in the width direction of the bearing according to the temperature at 3000RPM when the eccentricity is 0.9.....	51
Figure 3.19: Volume fraction at the bearing surface with temperature	52
Figure 3.20: Force and attitude angle according to temperature	53

Figure 3.21: Pressure field according to rotating speed changes at 50°C for eccentricity is 0.6	55
Figure 3.22: Pressure field according to rotating speed changes at 50°C for eccentricity is 0.8	56
Figure 3.23: Pressure field according to rotating speed changes at 50°C for eccentricity is 0.9	57
Figure 3.24: Plane view when projecting in the circumferential direction of the bearing.....	58
Figure 3.25: Circumferential pressure data applied to the bearing.....	58
Figure 3.26: Plane view when projection in the width direction of the bearing.....	60
Figure 3.27: Volume fraction of the gaseous lubricant in the width direction of the bearing according to the rotating speed at 50°C when the eccentricity is 0.6.....	60
Figure 3.28: Volume fraction of the gaseous lubricant in the width direction of the bearing according to the rotating speed at 50°C when the eccentricity is 0.8.....	61
Figure 3.29: Volume fraction of the gaseous lubricant in the width direction of the bearing according to the rotating speed at 50°C when the eccentricity is 0.9.....	61
Figure 3.30: Volume fraction at the bearing surface with temperature	62

Figure 3.31: Force and attitude angle according to rotation speed.....	63
Figure 3.32: Schematic of the bearing flow field with simple dimple structure.....	65
Figure 3.33: Comparison of pressure field and volume fraction with and without dimple structure	66
Figure 3.34: Pressure field according to dimple parameter changes at 50°C, 3000 RPM for eccentricity 0.8.....	68
Figure 3.35: Volume fraction of the gaseous lubricant of the dimple parameter changes at 50°C, 3000 RPM for eccentricity 0.8.....	69
Figure 3.36: Force, attitude angle and average load area according to dimple structure pattern	70



List of Tables

Table 3.1: Bearing dimensions and operating parameters	35
Table 3.2: Properties of Turbine oil 30	42
Table 3.3: Dimple parameters	64



Contents

Contents

Acknowledgement	v
List of Figures	vii
List of Tables	xi
Contents	xii
Chapter 1	1
1. Introduction	1
1.1. Research background	1
1.2. Literature review	2
1.3. Research purpose	7
Chapter 2	8
2. Comparative evaluation of basic theory and KS standard	8
2.1. CFD technique	8
2.2. Governing equations and turbulence model	9
2.2.1. Statistical turbulence models and the closure problem	10
2.2.2. Reynolds Averaged Navier Stokes (RANS) equations	11
2.2.3. Eddy viscosity turbulence models	13
2.2.4. K- ω model in CFX	15
2.2.4.1. Wilcox k- ω model	16
2.3. Journal bearing basic theory and design according to KS standard	18
2.3.1. Journal bearing basic theory	18

2.3.2. Journal bearing design according to KS standard	24
Chapter 3	32
3. Numerical Analysis	32
3.1. Numerical analysis modeling	32
3.1.1. Grid dependency test	35
3.1.2. Validation	38
3.2. Computational flow analysis according to viscosity change	40
3.2.1. Flow field analysis	44
3.2.1.1. Pressure field	44
3.2.1.2. Volume fraction of gaseous lubricant	49
3.2.2. Comparison of force and attitude angle	53
3.3. Computational flow analysis based on rotational speed	54
3.3.1. Flow field analysis	54
3.3.1.1. Pressure field	54
3.3.1.2. Volume fraction of gaseous lubricant	59
3.3.2. Comparison of force and attitude angle	62
3.4. Introduction of dimple structure to investigate bearing performance	63
3.4.1. Assessment of dimple effect	64
3.4.2. Effect of change of dimple parameters	67
4. Conclusions	72
5. References	74

Chapter 1

1. Introduction

1.1. Research background

A bearing is a mechanical element that supports the rotation of the shaft while supporting the load of the shaft. The types of bearing can be classified into rolling bearings and sliding bearings. Rolling bearings are bearings that support the rotation of the shaft due to rolling contact and support the load by introducing balls or rollers between the shafts and bearings. Sliding bearings have high viscosity lubricant between the shafts and bearings. It is a mechanical element that supports the rotation of the shaft and supports the load by lubrication. The sliding bearings has less friction because the friction is only related to the viscosity of the lubricant when the shaft has a proper number of rotations (rotating speed). Unlike rolling bearings with point or line contact, the sliding bearings are used for high speed and high loads because they have surface contact.

In the case of fuselage of automobiles or aircrafts that require high reliability, increased strength etcetera, the cold rolling process is used due to its effect of improved surface finish. On the other hand, the hot rolling process – which requires less load, less eccentricity – cannot be used for the cases of fuselage of automobiles or aircrafts due to its rough surface finish. Owing to high load and high eccentricity between the shaft and the center of the bearing, there are phenomena such as oil film destruction and excessive wear, as well as

journal destruction, which not only reduces the production efficiency due to the replacement of parts, but also due to economical loss of parts.

The limiting operating conditions for preventing journal bearing failure are determined by design criteria such as minimum oil film thickness for oil film formation, maximum temperature of the bearing, and stability characteristics to prevent unstable vibration of the bearing. In journal bearings, the shaft has a corresponding eccentricity and attitude angle so that the reaction force due to hydraulic pressure and the weight of the shaft are balanced during operation, thereby changing the film thickness. Therefore, predicting the temperature and pressure inside the bearing by analyzing the flow field of the lubricant can help reduce bearing damage.

1.2. Literature review

Journal bearings have been continuously researched and developed since the 1960s. Susilowati et al [1] made a comparative study of finite journal bearing in laminar and turbulent regimes using CFD techniques. They varied the sliding velocity from 3000, 5000 and 10000. Their results showed that the distribution of static hydrodynamic pressure was of similar trend for both the laminar and turbulent regimes. Also, the static pressure was low at the beginning of the contact and gradually increased to the maximum and then dropped significantly. Aksoy and Aksit [2] developed a coupled thermo-elastohydrodynamics model to predict the 3-D thermal, structural and hydrodynamic performance of foil bearing. The results show that due to the increasing shear heating effect on the thin film the temperature increased rapidly along with the shaft speed. They observed that the operation capability at very high speeds of the foil bearing is possible only with an advanced cooling

mechanism without which the bearing cannot operate at high speeds. Farrall et al [3] numerically studied the motion of an oil film flow in an aero-engine bearing chamber using the steady state, three dimensional, isothermal calculations. The results showed that the distribution of film thickness around the chamber housing is sensitive to the boundary condition imposed at the scavenge port. Raimondi and Boyd [4] studied the solution for finite journal bearing with its application to analysis and design. The results showed that larger film thickness was obtained for partial bearing calculations based on film rupture and for calculations based on no film rupture lower coefficients of friction were obtained. Dai and Khonsari [5] studied about the hydrodynamic lubrication of mixture of two fluids by deriving the governing equation. They showed that the volume fraction of the non-Newtonian fluid played an important role on the performance of the bearing. Andrade [6] studied about the theory of viscosity of liquids. Dhande and Pande [7] numerically studied the two-way FSI analysis of multiphase flow in hydrodynamic journal bearing with cavitation. The results showed a drop in maximum pressure value when cavitation is considered. Also, with an increase in shaft speed, the oil vapor distribution rises which lowers the magnitude of the pressure build up. Richard Armentrout et al [8] analyzed the turbulence and convective inertia in a water-lubricated tilting-pad journal bearing using the conventional and CFD approaches. The results showed that turbulence accounts for around 50% of the load capacity whereas convective inertia lowered the load capacity by about 6% when compared to an inertialess solution. Qiyin Lin et al [9] studied the lubrication performances of journal bearing system using CFD and FSI considering thermal influence and cavitation. They analyzed four journal bearings with different grooves to select suitable bearings that can be used in

high-speed rotor-bearing system. Their results showed that the eccentricity, temperature rise and pressure increased for an increase in the exerted external load. Also, for an increase in rotational speed, the temperature rise became higher and for an increase in the number of grooves, the temperature rise and cavitation volume fraction decreased linearly. Zenglin Guo et al [10] studied the analysis for rotating machinery using CFX-TASCflow to simulate the fluid-film bearing and damper designs. They studied the pressure field and calculated the static and dynamic characteristics of hydrodynamic, hydrostatic, hybrid bearings and squeeze film dampers using the CFX-TASCflow and compared the results with CFD analysis programs used in the industry. Constantinescu [11] studied the basic relationships in turbulent lubrication and their extension to include the thermal effects. Amir Jourak [12] studied the influence of textured rotor on journal bearing characteristics and the evaluation of CFD code capabilities to handle moving objects in the flow. The results showed that there was no numerical difference between a single and two geometries. Also, there was no increase in load carrying capacity of the journal bearing for a comparison between the textured and smooth rotor. Gertzos et al [13] numerically studied the journal bearing hydrodynamic lubrication by Bingham lubricant. The performance characteristics of the Bingham lubricated hydrodynamic journal bearing was derived by 3D CFD analysis and the results were compared to that of experimental and analytical data. Their results were found to be in good agreement. Gao Gengyuan et al [14] numerically studied the load carrying capacity of hydrodynamic lubrication on a water-lubricated journal bearing by a new bearing bush, with a transition-arc structure. Manshoor et al [15] studied the characteristics of a thin film lubricated plain journal bearing using 3D CFD analysis. They considered three turbulence models – namely, standard k-epsilon

model, realizable k-epsilon model and the Reynolds stress model to simulate the characteristics of the journal bearing. The results showed that all the models gave similar results in terms of performance. Yong and Balendra [16] conducted a CFD analysis on the lubrication behaviors of journal bearing with dimples, where the textured surface with dimple moves. The results showed that for the textured surface sliding, the friction force and friction coefficient were small when compared to the smooth surface sliding. Also, the increase in dimple depth and density resulted in decrease of friction force. Uhkoetter et al [17] studied about the development and validation of a 3D multiphase flow CFD analysis for journal bearings in steam and heavy duty gas turbines. The results showed that the CFD analysis was in good agreement with the experimental data. Jun Sun and Changlin [18] studied the hydrodynamic lubrication of journal bearing considering the misalignment caused by shaft deformation. They calculated the film pressure, load carrying capacity, attitude angle, and leakage flow rate, etc. for various misalignment degrees and eccentricity ratio. The results showed that the interaction effect between mechanical behavior of the shaft and journal bearing should be considered. Nengjun Jiang et al [19] analyzed about the improvement of journal bearing design using Numerical methods by studying the force direction and magnitude of 2D journal bearing and tapered gap and also the load of 3D journal bearing for different eccentric ratios. The numerical results were found to be in good agreement with the theoretical analysis results. Ermolaev et al [20] investigated about the vapor pressures of lubricating oils from 20 to 200 degree Celsius. The results showed that the degree of contamination of process gases depends on the oil grade and temperature. The theory of lubrication and its application was studied by Osborne Reynolds [21]. Fouflias et al [22] made a performance comparison study of bearings using CFD

thermohydrodynamics analysis. Four types of sector-pad thrust bearings – namely, an open pocket bearing, a closed pocket bearing, a tapered-land bearing and a bearing of partially textured with rectangular dimples – were considered. The results showed that the open pocket bearing had a superior performance when compared to the other bearing types. Kvitnitsky et al [23] studied the solution of Reynolds equation under natural boundary conditions for hydrodynamic journal bearings. The results showed that for Reynolds equation under natural boundary conditions, it was possible to obtain greater accuracy. Orcutt and Arwas [24] studied the steady state and dynamic characteristics of a full circular and partial arc bearing in laminar and turbulent flow regimes. Mukesh et al [25] studied the thermohydrodynamic analysis of a journal bearing using CFD techniques. Amit Singla et al [26] numerically studied the thermohydrodynamic analysis on temperature profile of circular journal bearing. The results showed that the temperature rise was less for the thermodynamic analysis when compared to the isothermal analysis. Sang Myung Chun [27] studied the thermohydrodynamic lubrication analysis of high speed journal bearing with variable density and variable specific heat considerations. The results showed that for the high shaft speed operations, the variable density and variable specific heat considerations cannot be ignored. Also, the calculated temperature may appear excessive to that of the real temperature if the real density and specific heat are not considered at higher shaft speed. Hanoca and Ramakrishna [28] numerically studied the effects of oil film thickness at the entrance of the infinitely long slider bearing. The results showed that low load carrying capacity and high frictional losses occur when the bearing operates below maximum load carrying capacity.

1.3. Research purpose

The purpose of this study is to analyze the characteristics of bearings through a sophisticated and detailed three-dimensional thermal and flow analysis of the entire bearing system, and to evaluate the bearing performance after suggesting a lubricating structure for performance improvement. An accurate method of predicting the temperature and pressure of a bearing is used as a very important tool in bearing design and can greatly contribute to performance improvement. As a bearing design that can be operated in an increasingly extreme environment is required, various and extensive parametric studies can ultimately be used as an important tool in designing high-speed, high-load, high-temperature, high-performance of bearing.

In this numerical study, a plain bearing is analyzed and a parametric study on this plain bearing is conducted for load sustainability. The performance of the plain bearing is evaluated. Also, a bearing with dimple structures are analyzed parametrically and its performance is compared with that of the plain bearing.

This study focuses on:

1. KS B ISO 7902 1~3 [29] and one-dimensional analysis of general bearing-related equations to identify characteristics of lubrication.
2. CFD technique using 3D Navier-Stokes equation analyzing the flow field inside the bearing.
3. Lubrication structure for improving bearing performance in high-load, high-speed bearings is presented and performance is evaluated and analyzed.

Chapter 2

2. Comparative evaluation of basic theory and KS standard

2.1. CFD technique

Computational Fluid Dynamics (CFD) is a computer-based analysis of Navier-Stokes equation, a nonlinear partial differential equation describing fluid phenomena, through various differential methods. In general, the commercial codes (such as ANSYS CFX) are based on the Finite Volume Method (FVM), which takes an integral for each finite volume and constructs and approximates the correlation of the physical quantities between adjacent finite volumes. It works well with the Semi-Implicit Method for Pressure Linked Equations (SIMPLE) technique that can solve the problem efficiently, as well as the compressive flow problem that needs to be solved by concentrating the lattice on the wall or the convergence characteristics at high Reynolds number.

Numerical analysis is usually carried out in three stages as shown in figure 2.1: Pre-Processing, Solver (calculation), and Post-Processing. In the pre-processing step, geometrical definition (calculation area) of the analysis area is performed to generate shapes and grids. The solver stage is a process of settings and analysis, where the appropriate numerical model and boundary conditions for the analysis are set and the arithmetic equation is solved by the iterative method. Finally, in the post-processing step, the analysis results are visualized.

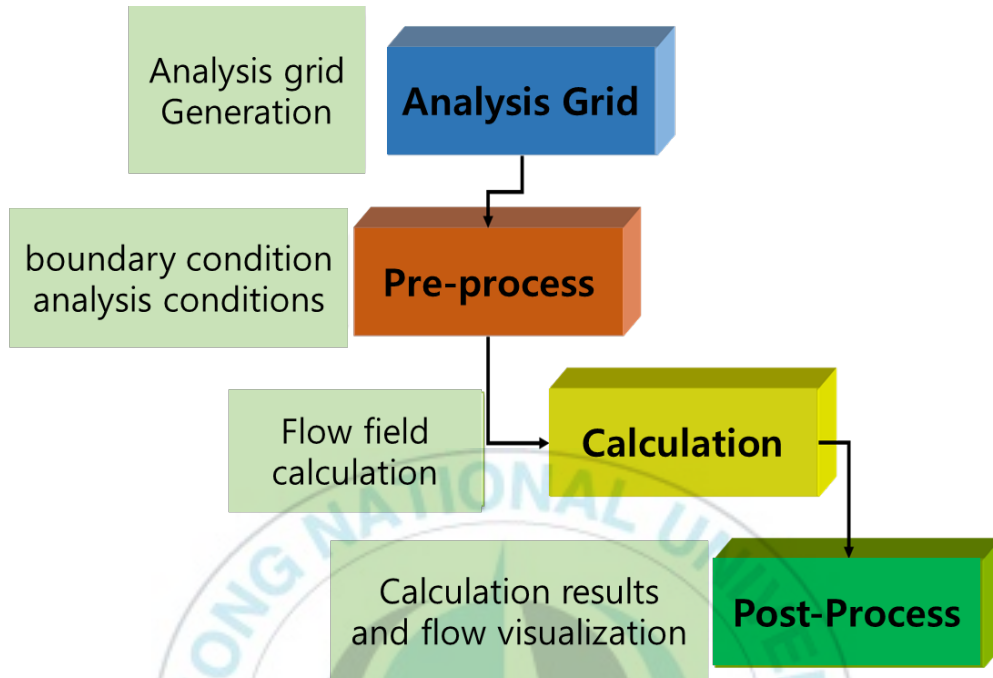


Figure 2.1: CFD interpretation process

2.2. Governing equations and turbulence model

Turbulence is caused by fluctuations in the flow domain over space and time, and is mainly three-dimensional, unsteady and has many flow scales. Turbulence has a significant effect on the properties of the flow and occurs when the inertial force in the flow is significantly greater than the viscous force, that is, when the Reynolds number is large.

The Navier-Stokes equation does not require additional information and describes both the turbulent and laminar flow. However, in actual Reynolds numbers, the length and time scale of turbulence vary widely and generally include a length scale smaller than the smallest control volume available for

numerical analysis. This flow is only possible in the future because it requires significant computer performance to interpret it as Direct Numerical Simulation (DNS).

To analyze the effects of turbulence, many CFD techniques, using turbulence models have been developed. In particular, the turbulence model was developed to account for the effects of turbulence of the DNS or computation using a fine mesh separately. Most turbulence models are derived through a statistical approach. The commercial code ANSYS CFX uses a turbulence model with a different approach. CFX provides Large Eddy Simulation (LES) model and a Detached Eddy Simulation (DES) model.

2.2.1. Statistical turbulence models and the closure problem

When the turbulence is averaged over a time scale that is much larger than the time scale of turbulence, an additional disturbance component that changes with time is produced. For example, the velocity component can be divided into an average component and a component that changes over time. The Reynolds Averaged Navier-Stokes (RANS) equations can be obtained by time-averaging the original unsteady Navier-Stokes equations using the mean and fluctuating components. In this process, all turbulence scales are included in the modeling. The RANS-based turbulence model is known as a statistical turbulence model because it undergoes a statistical averaging process to obtain the equation.

The analysis using the RANS equation saves a lot of computation time when compared to the DNS model and hence it is often used in the analysis of real engineering problems. However, in the averaging process, an additional unknown term occurs, which is expressed as the product of the fluctuating

component and acts as an additional stress term in the fluid. Therefore, this term is called ‘turbulent’ or ‘Reynolds stress’, and since it is difficult to solve directly it becomes a new unknown term. As a result, the number of unknowns is greater than the number of equations and hence an additional equation is needed to solve the problem. This problem is called as a 'closure' problem. In order to solve the closure problem, the process of modeling the Reynolds stress term as an average component is a turbulence model and the turbulence model is classified according to the type of the equation used.

2.2.2. Reynolds Averaged Navier Stokes (RANS) equations

The turbulence model is a means to solve the modified transport equation by introducing the mean and variance components. For example, the velocity U can be divided into the average component \bar{U} and the variable component u over time.

$$U = \bar{U} + u \quad (2.1)$$

Here,

$$\bar{U} = \frac{1}{\Delta t} \int_t^{t+\Delta t} U dt$$

where Δt is a time scale that is relatively larger than the turbulence fluctuation scale, but a time scale that is smaller than the total time to solve the equation.

Substituting the time-averaged physical quantity into the original transport equation, the following RANS equation can be obtained.

$$\frac{\partial \rho}{\partial t} + \nabla \cdot (\rho U) = 0 \quad (2.2)$$

$$\frac{\partial \rho U}{\partial t} + \nabla \cdot (\rho U \otimes U) = \nabla \cdot (\tau - \rho \overline{u \otimes u}) + S_M \quad (2.3)$$

where τ is the molecular stress tensor.

$$\frac{\partial \rho \phi}{\partial t} + \nabla \cdot (\rho U \phi) = \nabla \cdot (\Gamma \nabla \phi - \rho \overline{u \phi}) + S_E \quad (2.4)$$

The continuous equation is unchanged, but the momentum and scalar transport equations include the Reynolds stress term $\rho \overline{u \otimes u}$ and the Reynolds flow rate $\rho U \phi$. These terms appear from nonlinear convection terms in the non-averaging equation. These terms indicate that convection by turbulent velocity fluctuation is greater than the mixing caused by thermal fluctuation at the molecular level. At high Reynolds numbers, turbulent velocity fluctuations have a length scale much greater than the mean free path of thermal fluctuations. Thus, the turbulent flow rate becomes much greater than the molecular flow rate.

The Reynolds Averaged Energy equation is

$$\frac{\partial \rho h_{tot}}{\partial t} + \nabla \cdot (\rho U h_{tot} + \rho \overline{u h} - \lambda \nabla T) = \frac{\partial \rho}{\partial t} \quad (2.5)$$

Here, the averaged total enthalpy is given by

$$h_{tot} = h + \frac{1}{2} U^2 + k \quad (2.6)$$

Total enthalpy includes mean kinetic energy and turbulent kinetic energy. Here, turbulent kinetic energy is defined as follows.

$$k = \frac{1}{2} \overline{u^2} \quad (2.7)$$

The turbulence model serves to close the Reynolds averaged equation by providing a model for the calculation of Reynolds stress and Reynolds flow rates. The turbulence model provided by ANSYS CFX can be roughly divided into two types: Eddy viscosity models and Reynolds stress models.

2.2.3. Eddy viscosity turbulence models

The Eddy viscous model consists of small Eddies in which the turbulence continuously forms and dissipates, and the Reynolds stress in the vortex is proportional to the average velocity gradient. The viscous assumptions, similar to the relationship between stress and strain in Newtonian fluids, assumes a gradient of mean velocity and an Eddy viscosity using a gradient diffusion hypothesis.

$$-\rho \overline{u \otimes u} = -\frac{2}{3} \rho k \delta - \frac{2}{3} \mu_t \nabla \cdot U \delta + \mu_t (\nabla U + \nabla(U)^T) \quad (2.8)$$

where μ_t is the Eddy viscous or turbulent viscous and is the value to be determined.

Similar to the Eddy viscous, the Eddy diffusion implies that the Reynolds flow rate of a scalar is linearly proportional to the mean scalar gradient.

$$-\rho \overline{u\phi} = \Gamma_t \nabla \phi \quad (2.9)$$

where Γ_t is the Eddy diffusion coefficient expressed as

$$\Gamma_t = \frac{\mu_t}{Pr_t} \quad (2.10)$$

where Pr_t is the turbulent Prandtl number.

In order to solve the above equations, information on turbulent viscosity μ_t is required. The turbulent viscosity can be defined through a two-equation turbulence model such as $k - \varepsilon$ and $k - \omega$. According to the assumptions mentioned above, the Reynolds Averaged Momentum equation and the scalar transport equation are expressed as

$$\frac{\partial \rho U}{\partial t} + \nabla \cdot (\rho U \otimes U) = B - \nabla p' + \nabla \cdot (\mu_{eff} (\nabla U + (\nabla U)^T)) \quad (2.11)$$

$$\frac{\partial \rho \phi}{\partial t} + \nabla \cdot (\rho U \phi - \Gamma_{eff} \nabla \phi) = S \quad (2.12)$$

where B is the sum of body force, μ_{eff} is the effective viscosity and Γ_{eff} is the effective diffusivity, defined as:

$$\mu_{eff} = \mu + \mu_t \quad (2.13)$$

$$\Gamma_{eff} = \Gamma + \Gamma_t \quad (2.14)$$

Here, p' is the correction pressure.

$$p' = p + \frac{2}{3}\rho k + \nabla \cdot \mathbf{U} \left(\frac{2}{3}\mu_{eff} - \zeta \right) \quad (2.15)$$

where ζ is the bulk viscosity.

The Reynolds averaged energy equation is

$$\frac{\partial(\rho h_{tot})}{\partial t} - \frac{\partial P}{\partial t} + \nabla \cdot (\rho \mathbf{U} h_{tot}) = \nabla \cdot \left(\lambda \nabla T + \frac{\mu_t}{Pr_t} \nabla h \right) + S_E \quad (2.16)$$

If the enthalpy depends on a variable other than temperature, the modified molecular diffusion term is inaccurate, but the turbulent diffusion term due to diffusion assumption is accurately expressed. Moreover, turbulent diffusion is generally much larger than molecular diffusion, so the error by the latter can be neglected. The Reynolds averaged transport equation including the added variables is given by

$$\frac{\partial \rho \Phi}{\partial t} + \nabla \cdot (\rho \mathbf{U} \Phi) = \nabla \cdot \left(\Gamma_\phi + \frac{\mu_t}{\sigma_\phi} \right) \nabla \Phi + S \quad (2.17)$$

2.2.4. K- ω model in CFX

One advantage of the k- ω model is that it can effectively compute the low Reynolds number region near the wall. This model has excellent accuracy

and reliability without using the complex nonlinear damping function used in the k- ϵ model. Low Reynolds number k- ϵ models typically requires near-wall resolution of $y^+ < 0.2$, whereas k- ω models require at least $y^+ < 2$. It is difficult to guarantee even $y^+ < 2$ in the flow covered by the field. For this reason, a new method was developed for the k- ω model. This method enables smooth transition from low Reynolds number form to wall function.

The k- ω model defines turbulent viscosity as

$$\mu_t = \rho \frac{k}{\omega} \quad (2.18)$$

2.2.4.1. Wilcox k- ω model

In this study, the k- ω model, proposed by Wilcox is used. It uses the turbulent kinetic energy k, turbulent frequency and ω equation. The stress tensor is calculated from the Eddy viscosity.

k-equation:

$$\frac{\partial(\rho k)}{\partial t} + \nabla \cdot (\rho U k) = \nabla \cdot \left[\left(\mu + \frac{\mu_t}{\sigma_k} \right) \nabla k \right] + P_k - \beta' \rho k \omega \quad (2.19)$$

ω -equation:

$$\frac{\partial(\rho \omega)}{\partial t} + \nabla \cdot (\rho U \omega) = \nabla \cdot \left[\left(\mu + \frac{\mu_t}{\sigma_\omega} \right) \nabla \omega \right] + \alpha \frac{\omega}{k} P_k - \beta' \rho \omega^2 \quad (2.20)$$

In this model, the constants used in the calculation are as follows. $\beta' = 0.09$, $\alpha = 5/9$, $\beta = 0.075$, $\sigma k = 2$, $\sigma \omega = 2$. The unknown Reynolds stress tensor τ is calculated from the following equation

$$\tau = \mu_t 2s - \rho \frac{2}{3} \delta k \quad (2.21)$$

To avoid the formation of turbulent kinetic energy in the stagnation region, Menter [30] used the following limiter in the turbulent kinetic energy generation term:

$$\widetilde{P}_k = \min(P_k, c_{lim} \varepsilon) \quad (2.22)$$

Here, $c_{lim} = 10$. The limiter does not affect the model's shear layer computational performance, but it prevents the formation of stagnation points in aerodynamic simulation.

2.3. Journal bearing basic theory and design according to KS standard

2.3.1. Journal bearing basic theory

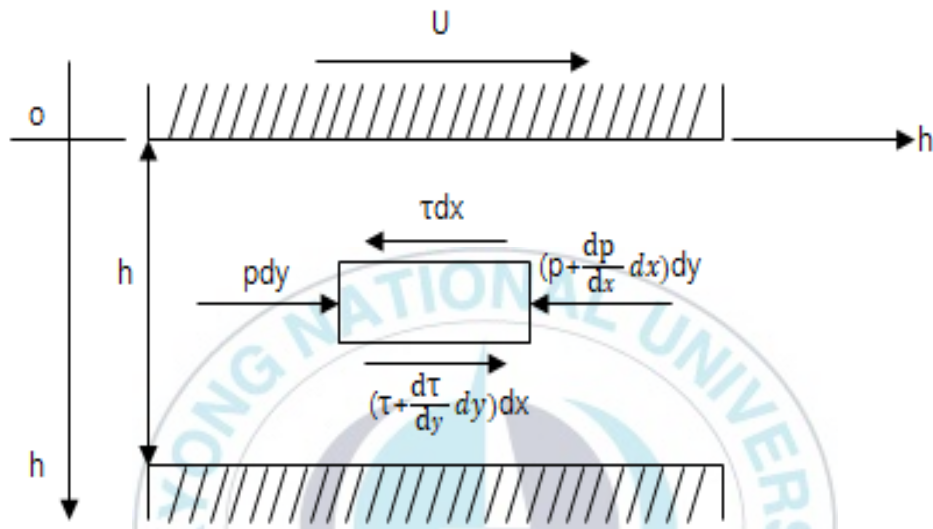


Figure 2.2: Shear force between two planes

Figure 2.2 shows the shear force between the two planes. The sliding between the two planes causes most of the fluid to shear the x -direction. The following assumptions are made to simplify the theoretical analysis.

1. The lubricant follows Newton's law of viscosity.
2. The inertial force of lubricant is considered to be negligible and hence ignored.
3. The lubricant oil is incompressible
4. The viscosity coefficient of the lubricant is constant
5. The pressure of the fluid in the y -direction is constant.

Therefore, using the boundary conditions $y = 0, u = U, y = h$, and $u = 0$ in the force equilibrium, the Reynolds equation for a one-dimensional flow can be obtained as follows.

$$\frac{d}{dx} \left(\frac{h^3}{\eta} \frac{dp}{dx} \right) = 6U \frac{dh}{dx} \quad (2.23)$$

If considering the flow in the z-direction, the Reynolds equation based on the three-dimensional lubrication theory is given by

$$\frac{\partial}{\partial x} \left(\frac{h^3}{\eta} \frac{\partial p}{\partial x} \right) + \frac{\partial}{\partial z} \left(\frac{h^3}{\eta} \frac{\partial p}{\partial z} \right) = 6U \frac{dh}{dx} \quad (2.24)$$

Figure 2.3 shows the pressure distribution during the bearing operation. Sommerfeld derives the equation for obtaining the friction coefficient by geometric analysis of the actual sliding bearing with hydraulic distribution as shown in figure 2.3.

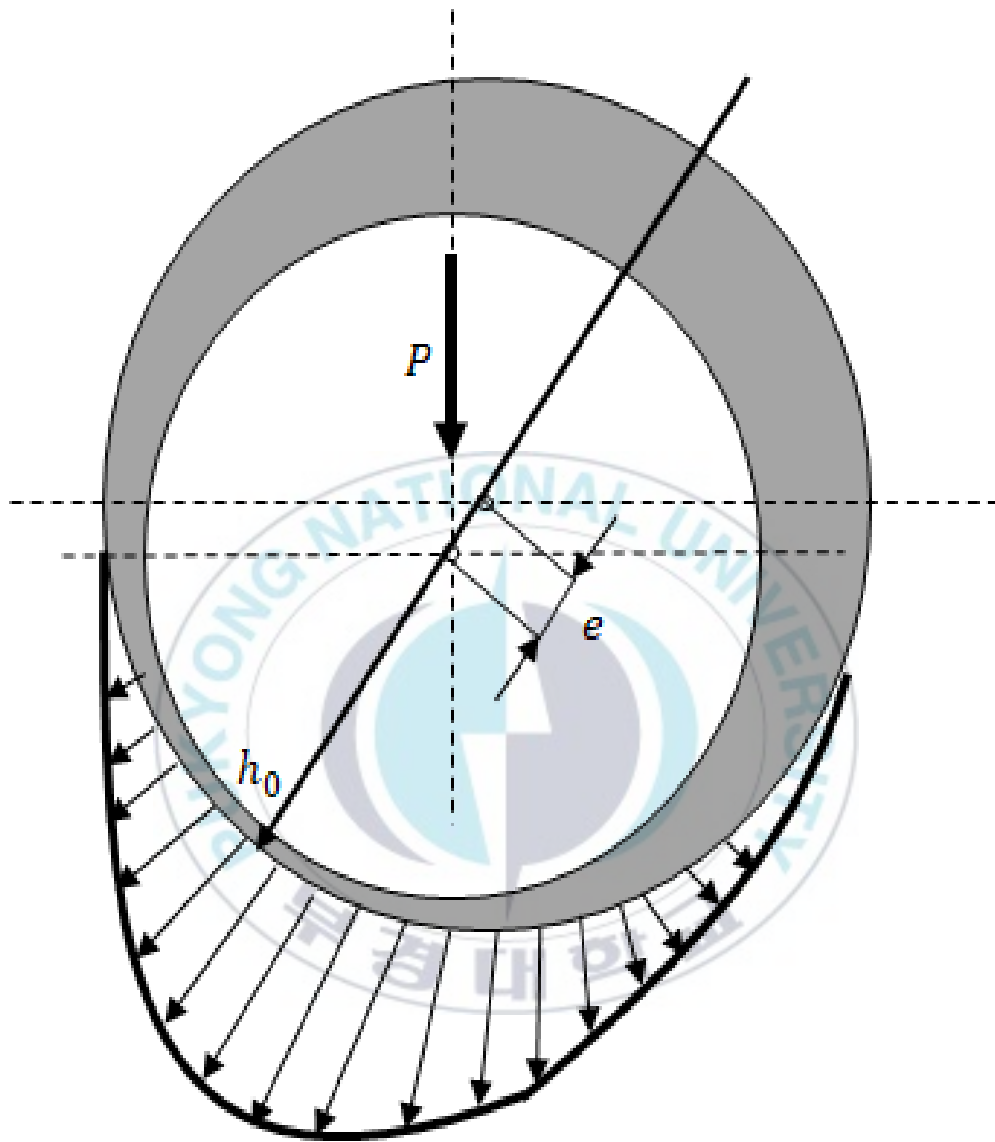


Figure 2.3: Pressure distribution during bearing operation

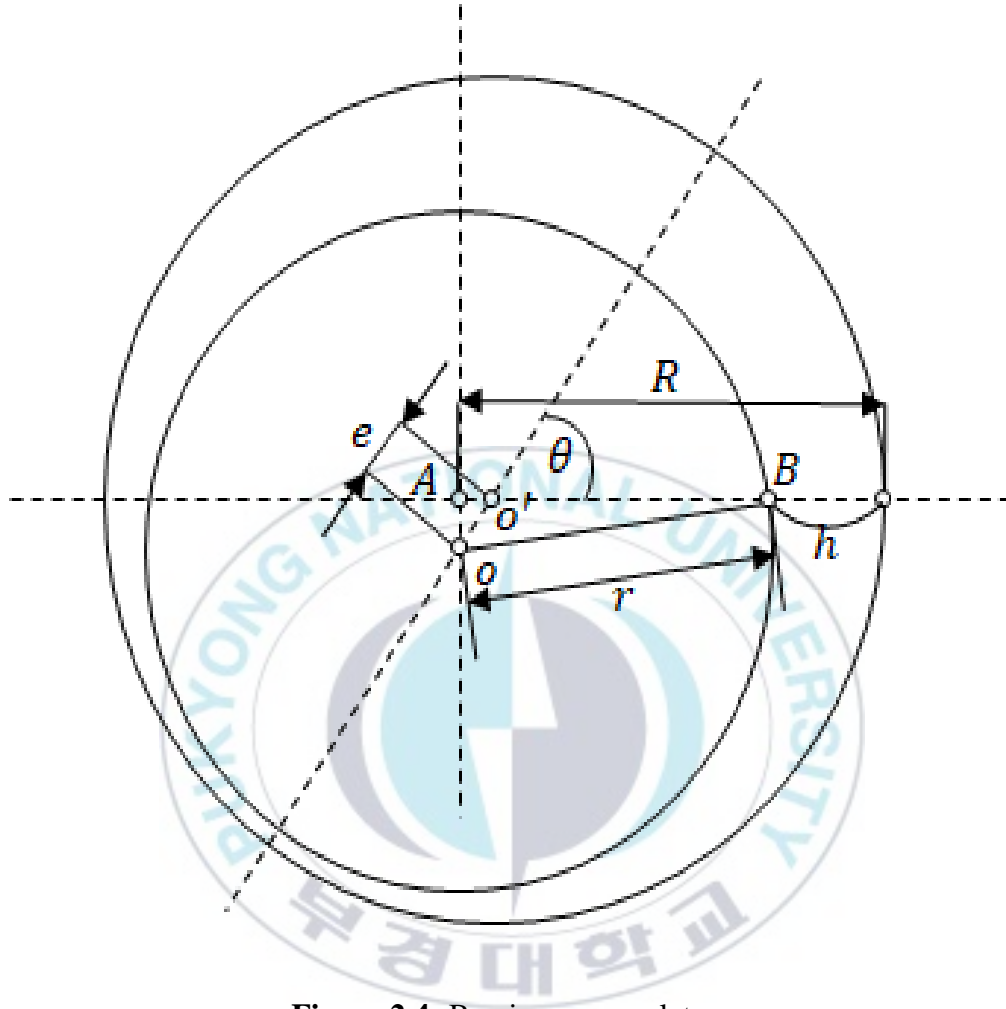


Figure 2.4: Bearing nomenclature

Figure 2.4 shows the bearing nomenclature. In the figure, O is the center of the shaft, O' is the center of the bearing, $\overline{OO'}$ is the line segment, e is the eccentricity, r is the radius of the shaft, R is the radius of the bearing, h is the thickness of the oil film and θ is the angle at arbitrary position. The thickness h of the oil film is given by

$$h = R - r + e \cos \theta = c + e \cos \theta = c(1 + n \cos \theta) \quad (2.25)$$

Here, the bearing radius clearance c and the eccentricity rate n are given by

$$c = R - r, \quad n = \frac{e}{c} \quad (2.26)$$

Therefore, the maximum thickness h_{max} and minimum thickness h_{min} of the oil film is as follows.

$$h_{max} = c + e = c(1 + n), \quad \text{when, } \theta = 0, 2\pi \quad (2.27)$$

$$h_{min} = c - e = c(1 - n), \quad \text{when, } \theta = \pi \quad (2.28)$$

Using $r d\theta \doteq dx$ and simplifying, the oil film pressure p is given by.

$$p = P_0 + \frac{6\eta U r}{c^2} \left[\frac{n(2 + n \cos \theta) \sin \theta}{(2 + n^2)(1 + n \cos \theta)^2} \right] \quad (2.29)$$

On the other hand, the load capacity P per unit width of the bearing is

$$P = \int_0^{2\pi} p r \sin \theta d\theta = \eta U \left(\frac{r}{c^2} \right) \left(\frac{12\pi n}{2 + n^2 \sqrt{1 - n^2}} \right) \quad (2.30)$$

And τ is the shear stress. The friction torque T per unit width acting on the shaft is

$$T = r^2 \int_0^{2\pi} r d\theta = \frac{\eta U r^2}{c} \left(\frac{4\pi(1 + 2n^2)}{(2 + n^2)(\sqrt{1 - n^2})} \right) \quad (2.31)$$

The friction coefficient at torque $T = \mu Pr$ is

$$\mu = \frac{T}{Pr} = \frac{c}{r} \left(\frac{1 + 2n^2}{3n} \right) \quad (2.32)$$

Rearranging, we get

$$\left(\frac{r}{c} \right)^2 \frac{\eta N}{p} = \frac{(2 + n^2)\sqrt{1 - n^2}}{12\pi^2 n} \quad (2.33)$$

In 2.33, if $\left(\frac{r}{c} \right)^2 \frac{\eta N}{p}$ is constant, then n is also a constant. Hence, the other characteristics of the bearing are determined as follows.

$$\frac{h_{min}}{c} = 1 - n, \quad \frac{r}{c} \mu = \frac{1 + 2n^2}{3n}, \quad \frac{r}{h_{min}} \mu = \frac{1 + 2n^2}{3n(1 - n)} \quad (2.34)$$

All bearing performance is a function of $\left(\frac{r}{c} \right)^2 \frac{\eta N}{p}$. And it is an important dimensionless quantity that determines the performance of bearings. This is called the Sommerfeld number and is expressed as S .

$$S = \left(\frac{r}{c} \right)^2 \frac{\eta N}{p} \quad (2.35)$$

2.3.2. Journal bearing design according to KS standard

This section describes a reliable design method according to the Korean Industry Standard for oil-lubricated plain bearings in which the shaft and the bearing surface are completely separated by an oil lubricating membrane. The crevice geometry is constant except for negligible deformations due to pressure and temperature of the lubricating film. The basis of the calculation is Reynolds equation for finite length bearings calculated with physically correct boundary conditions for the generation of pressure. A numerical solution of the Reynolds differential equation is given by

$$\frac{\partial}{\partial x} \left(h^3 \frac{\partial p}{\partial x} \right) + \frac{\partial}{\partial z} \left(h^3 \frac{\partial p}{\partial z} \right) = 6\eta(u_j + u_B) \frac{\partial h}{\partial x} \quad (2.36)$$

It is an ideal assumption that has been experimentally and practically verified, and the following prerequisites are used:

- a) The lubricant is a Newtonian fluid.
- b) All lubricant flow is laminar.
- c) The lubricant adheres completely to the sliding surface.
- d) The lubricant is incompressible.
- e) The loaded and unloaded regions of the bearing are completely filled with lubricant
- f) The inertial effects of lubricant, gravity and magnetic force are neglected.
- g) The components that form the clearances of the bearings are rigid or the deformation is negligible and the surface is an ideal cylindrical cylinder.

- h) The radius of curvature of the surfaces where relative motion occurs is greater than the thickness of the lubricant film.
- i) The thickness of the lubricant film in the axial direction (z-coordinate) is constant.
- j) Variations in the pressure of the lubricant in the direction perpendicular to the bearing surface (y-coordinate) are negligible.
- k) There is no movement in the direction perpendicular to the bearing surface (y-coordinate).
- l) The lubricant in the clearance has the same viscosity for the entire bearing.
- m) Lubricant is supplied at the starting point of the bearing liner or where the gap of the lubricant is the largest. The size of the lubricant supply pressure is negligible compared to the lubricant film pressure.

The following factors should be considered in the calculation of the plain bearing.

- a) The relationship between load carrying capacity and lubricating film thickness
- b) Friction loss power
- c) Lubricant flow rate
- d) Thermal equilibrium

All these factors are interrelated. The solution is obtained using the iterative method, and the sequence is shown in the flow chart figure 2.5.

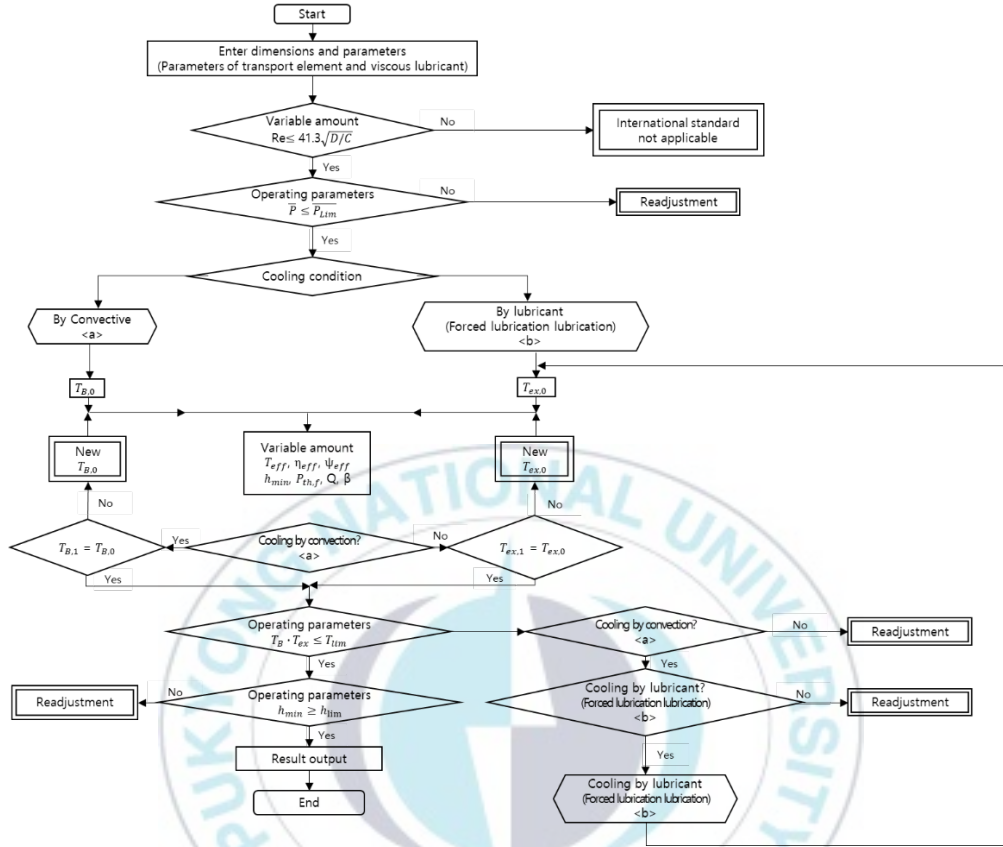


Figure 2.5: Flowchart of bearing characteristic calculation

Here, the Reynolds number inside the bearing lubricant flow field is given by:

$$Re = \frac{\rho U_j \frac{C_{R,eff}}{2}}{\eta} = \frac{\pi D N_j \frac{C_{R,eff}}{2}}{\nu} \leq 41.3 \sqrt{\frac{D}{C_{R,eff}}} \quad (2.37)$$

In the case of plain bearings, if $Re \geq 41.3 \sqrt{\frac{D}{C_{R,eff}}}$, then higher loss coefficient and bearing temperatures are expected. Calculations for turbulent bearings cannot be performed according to KS standard. The minimum lubricating film thickness, h_{min} is given by

$$h_{min} = \frac{D - D_J}{2} - e = 0.5D\psi(1 - \epsilon) \quad (2.38)$$

Here, the relative eccentricity ϵ is given by

$$\epsilon = \frac{e}{\frac{D - D_J}{2}} \quad (2.39)$$

The attitude angle ϕ_2 is given by

$$\phi_2 - (\pi - \beta) < \frac{\pi}{2} \quad (2.40)$$

Then

$$h_{min} = 0.5D\psi(1 + \epsilon \cos \phi_2) \quad (2.41)$$

The characteristic parameter for load-capacity is the dimensionless Sommerfeld number S_0

$$S_0 = \frac{F\psi_{eff}^2}{DB\eta_{eff}\omega_h} = S_0\left(\epsilon, \frac{B}{D}, \Omega\right) \quad (2.42)$$

Friction of plain bearings due to shear stress is given by the dimensionless property of friction power loss and ξ and f/ψ_{eff} is given by

$$\xi = \frac{F_f\omega_{eff}}{DB\eta_{eff}\omega_h} \quad (2.43)$$

$$\frac{f}{\omega_{eff}} = \frac{\xi}{S_0} \quad (2.44)$$

Equation 2.42 applies only when frictional power loss occurs in the load region of the lubricating film. However, it is necessary to calculate the frictional power loss in the load area and the no-load area, which means when the entire gap is filled with lubricant.

$$P_f = P_{th,f} = fF\left(\frac{D}{2}\right)\omega_h \quad (2.45)$$

Heat-related conditions for plain bearings can be obtained from thermal equilibrium. The heat flow $P_{th,f}$ from the frictional power P_f in the bearing is distributed to the surroundings through the bearing housing or through the lubricant discharged from the bearing. In practice, either heat dissipation is dominant. By ignoring other heat losses, additional safety margins can be secured at the design stage. The following assumptions are used.

a) Bearings without pressure generation (forced lubrication at the inlet) dissipate heat, mainly by convection. It is given by

$$P_{th,f} = P_{th, amb} \quad (2.46)$$

where, $P_{th,f}$ is heat dissipation and $P_{th, amb}$ thermal transfer due to ambient.

b) Pressure-generated bearings dissipate heat mainly by the lubricant. It is given by

$$P_{th,f} = P_{th,L} \quad (2.47)$$

where, $P_{th,f}$ is heat dissipation and $P_{th,L}$ thermal transfer due to lubricant.

For forced feed lubrication, heat dissipation through the lubricant is given by

$$P_{th,L} = \rho c Q (T_{ex} - T_{en}) \quad (2.48)$$

From the heat balance, the bearing temperature T_B and the lubricant outlet temperature T_{ex} can be found. The effective lubricating film temperature involved in lubricant viscosity are pure convection and heat dissipation through lubricant.

a) For pure convection

$$T_{eff} = T_B \quad (2.49)$$

b) For heat dissipation through lubricant

$$T_{eff} = \bar{T}_L = 0.5(T_{en} + T_{ex}) \quad (2.50)$$

When operating at high speed, a temperature that is slightly closer to the lubricant outlet temperature can be chosen instead of the average value.

The calculated values for T_B and T_{ex} should be checked for acceptance through comparison with a given tolerance range T_{lim} ([29]). Initial operating conditions T_{amb} or T_{en} are known, but the effective temperature T_{eff} required at the beginning of the calculation is unknown. The solution can be found by starting the calculation using the assumed temperature rise as follows.

$$T_{B,0} - T_{amb} = 20K \quad (2.51)$$

$$T_{ex,0} - T_{en} = 20K \quad (2.52)$$

In spherical cylindrical journal bearings with an eccentric shaft, the clearance h is given by

$$h = 0.5D\psi_{eff}(1 + \epsilon\phi) \quad (2.53)$$

The minimum lubricating film thickness is as follows

$$h = 0.5D\psi_{eff}(1 - \epsilon) \quad (2.54)$$

The specific bearing load is as follows

$$\bar{P} = \frac{F}{DB} \quad (2.55)$$

The bearing clearance during operation is due to the thermal expansion and fitting of the shaft and the bearing. The relative bearing clearance in the initial condition (20°C) is given by

$$\psi_{max} = \frac{D_{max} - D_{J,min}}{D} \quad (2.56)$$

$$\psi_{min} = \frac{D_{min} - D_{J,max}}{D} \quad (2.57)$$

$$\bar{\psi} = 0.5(\psi_{max} - \psi_{min}) \quad (2.58)$$

The variable to be determined in the calculation is the effective relative bearing clearance ψ_{eff} – at the effective lubricating film temperature T_{eff} – which is regarded as the average temperature of the bearing and shaft. When the shaft and the bearing have different coefficients of linear expansion, the thermal change of the relative bearing clearance is given as follows.

$$\begin{aligned} \Delta\psi &= (\alpha_{l,B} - \alpha_{l,J})(T_{eff} - 20^\circ\text{C}) \\ &= \alpha_{l,B}(T_B - 20^\circ\text{C}) - \alpha_{l,J}(T_S - 20^\circ\text{C}) \end{aligned} \quad (2.59)$$

$$\psi_{eff} = \bar{\psi} + \Delta\psi \quad (2.60)$$

Chapter 3

3. Numerical Analysis

3.1. Numerical analysis modeling

The friction state of a sliding bearing can be roughly divided into three types according to the operating conditions. In the initial condition, where the bearing is at rest – due to the load – it is in contact with the shaft. Also, it is in a solid or dry friction state without any lubricant between the contact surfaces. Since the friction coefficient has a value of 0.1 or higher, the frictional resistance is high and thus the heat and wear are severe. As the shaft starts to rotate, it moves inside the bearing and a lubricant flows between them due to the squeezing effect. Hence, due to viscosity of the lubricant a thin oil film is formed. During this stage, it can be said to be at a relatively frequent friction state because the boundary lubrication occurs and it is difficult to maintain complete fluid lubrication in the actual bearing. Finally, when the bearing attains proper rotational speed, eccentricity occurs in the opposite direction of rotation due to the wedge action of the shaft, and the contact surfaces of the two objects are completely separated. Since this friction is only related to the viscosity of the lubricant regardless of the material or condition of the contact surface, the friction coefficient has a value of 0.01 or less. Hence, it can be said to be the most ideal friction state.

In this study, the steady state was analyzed by assuming that the bearing reached an appropriate rotational speed, and it was also analyzed by assuming

that the lubricant was properly supplied between the shaft and the bearing and there was no change in the properties of the lubricant.

Figure 3.1 shows the bearing boundary conditions used in the numerical analysis. The bearing consists of a bearing wall, an inlet, a shaft (rotating wall) and an opening outlet at atmospheric pressure. When the lubricant enters the inlet at a pressure of 1 Bar, the lubricant rotates between the shaft and the bearing while the shaft rotates counterclockwise.

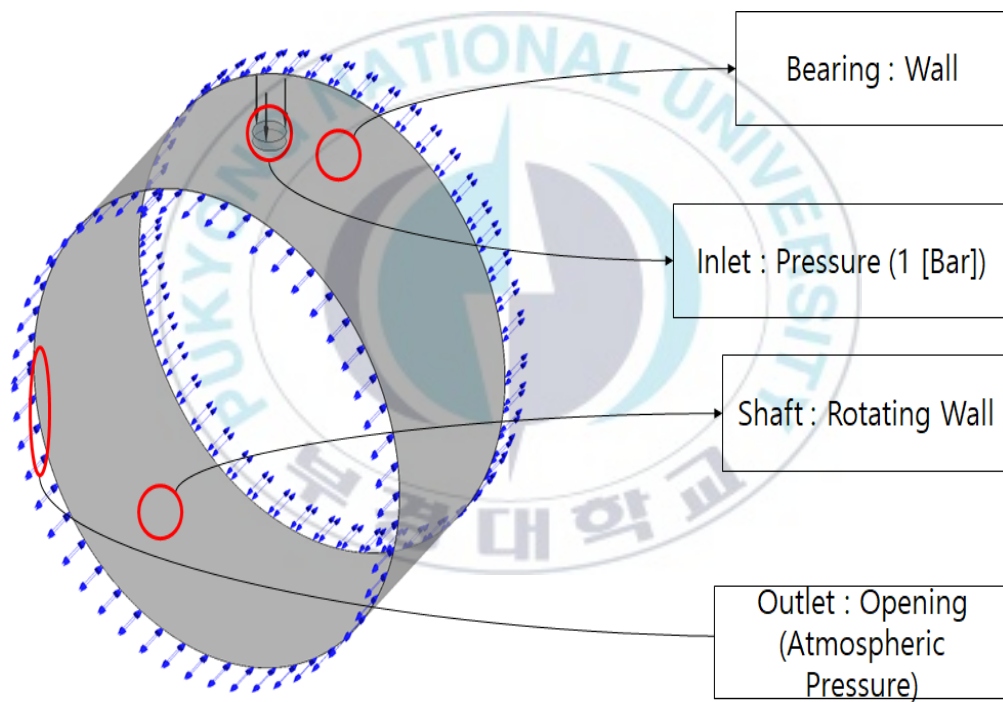


Figure 3.1: Bearing boundary conditions used in numerical analysis

Figure 3.2 shows the modeling process of the flow field of the journal bearing. The bearing consists of an oil inlet, housing, bearing liner, clearance,

split type and a journal or a shaft as shown in figure 3.2 (a). Figure 3.2 (b) shows the flow field of the journal bearing and figure 3.2 (c) shows the flow field model used for numerical analysis in this study. The clearance between the bearing and the shaft is filled with lubricant and modeled. Table 3.1 shows the bearing dimensions and operating parameters. In this study, the analysis was performed according to the rotation speed, lubrication temperature and eccentricity.

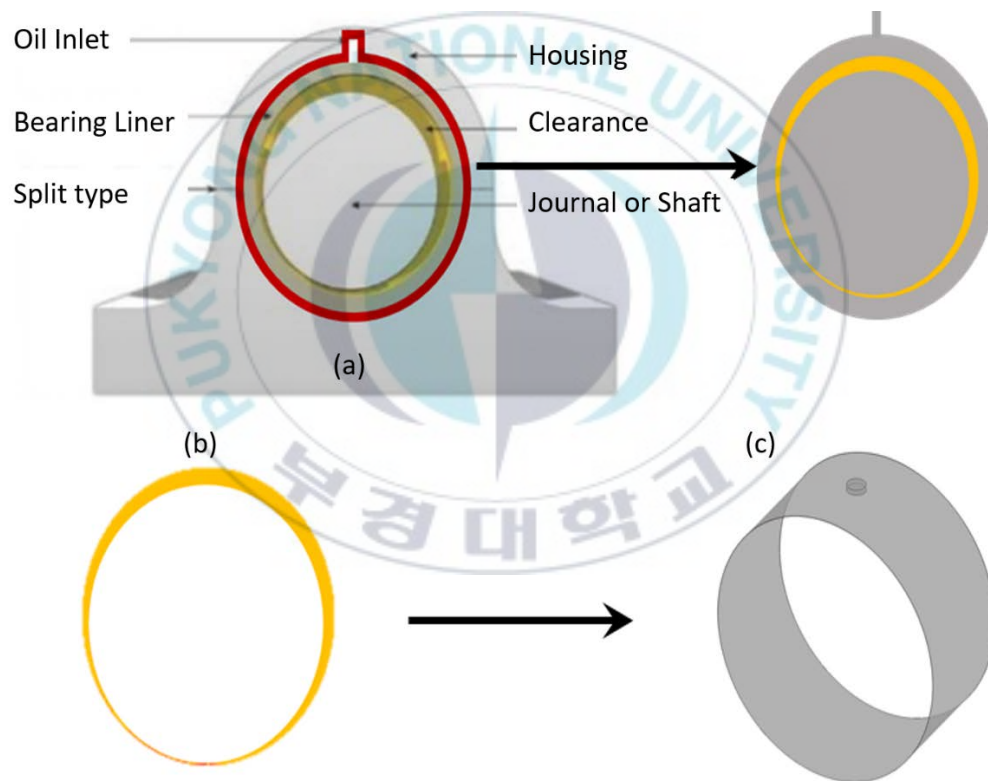


Figure 3.2: Modeling process of journal bearing flow field. (a) journal bearing; (b) flow field of journal bearing; (c) flow field model used for analysis

Table 3.1: Bearing dimensions and operating parameters

Parameter	Value
Shaft diameter, D	50 [mm]
Clearance, C	50 [μ m]
Length of the bearing, L	25 [mm]
Speed, N	1000, 2000, 3000, 4000, 5000 [RPM]
Temperature	50, 100, 150, 180, 200 [°C]
Lubricant density, ρ	850 [kg/m^3]
Eccentricity	0.6, 0.8, 0.9 ($\epsilon = \frac{\text{Center of Shaft} - \text{Center of Bearing}}{\text{Average lubrication thickness}}$)
Lubricant	Turbine oil – 30

3.1.1. Grid dependency test

Prior to comparing numerical analysis results with experimental results, it is necessary to minimize errors caused by improper lattices. The method of predicting the error caused by a coarse lattice system is to investigate the lattice dependence, that is, when starting from the most coarse lattice system and gradually constructing the lattice, the key variables are no longer changed, so the simulation results are displayed on the lattice. Thus the lattices become independent. In this study, the lattice dependence was confirmed by calculating the load of the shaft while increasing the number of lattices in the direction of the width, circumference, and lubrication thickness of the bearing, which is expected to have a change in flow.

Figure 3.3 shows the analysis results according to the number of mesh of lubrication thickness. Figure 3.4 shows the analysis results according to the number of mesh of bearing width direction. Figure 3.5 shows the analysis results according to the number of mesh of circumferential direction. From these figures, it can be seen that, when the number of grids is 20 in the lubricating thickness direction, 100 in the bearing width direction and approximately 1260 in the circumferential direction, the error is within 1 %. The total number of nodes is 3,111,763. Hexa meshes are generated and the commercial code ANSYS 18.2 [31] is used for the simulation.

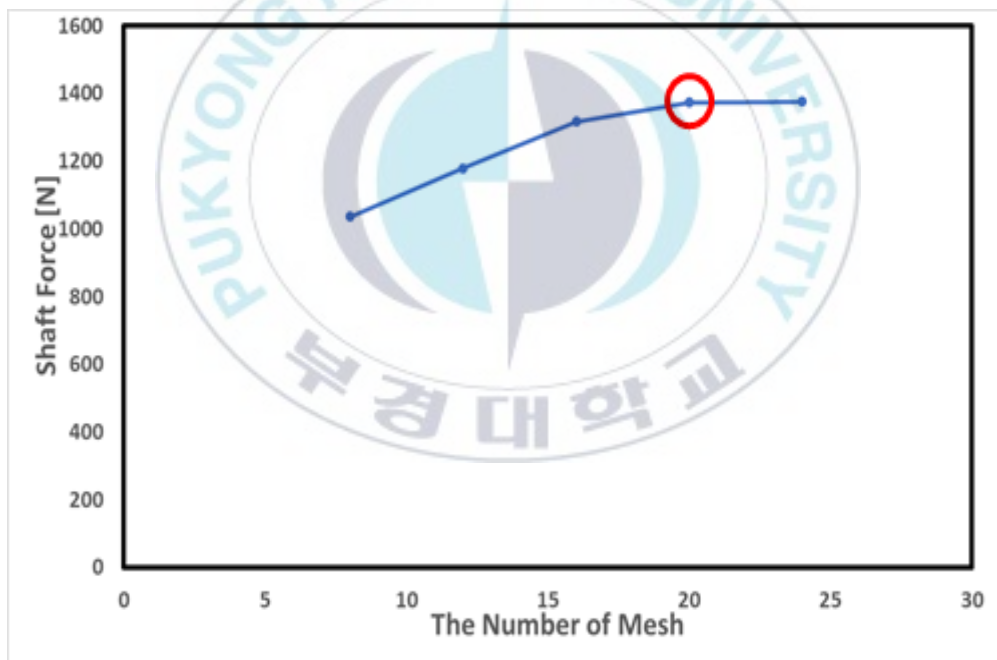


Figure 3.3: Analysis result according to the number of mesh of lubrication thickness

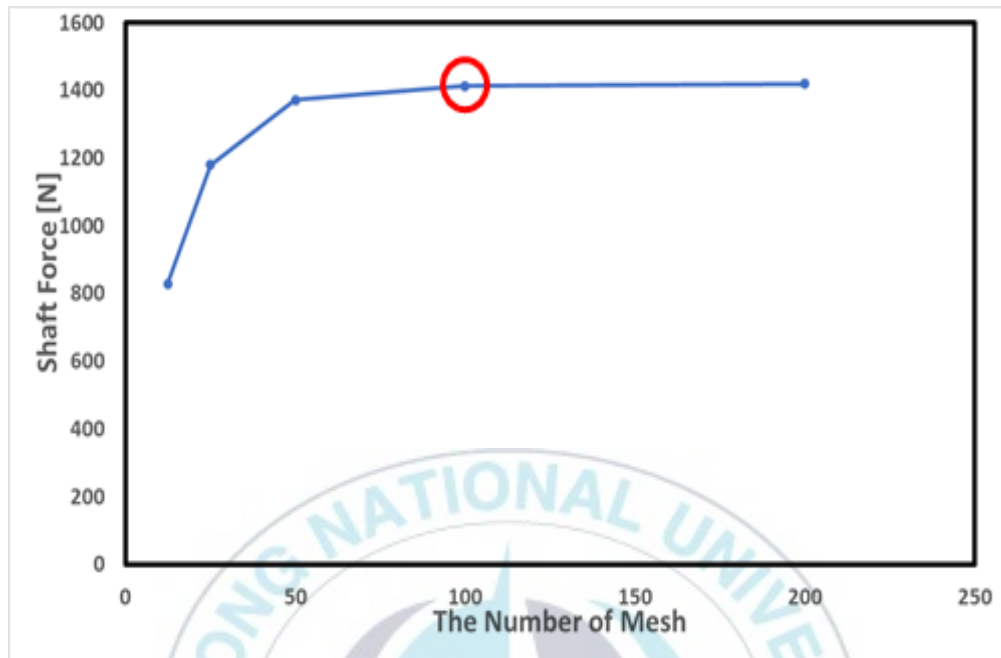


Figure 3.4: Analysis result according to the number of mesh of bearing width direction

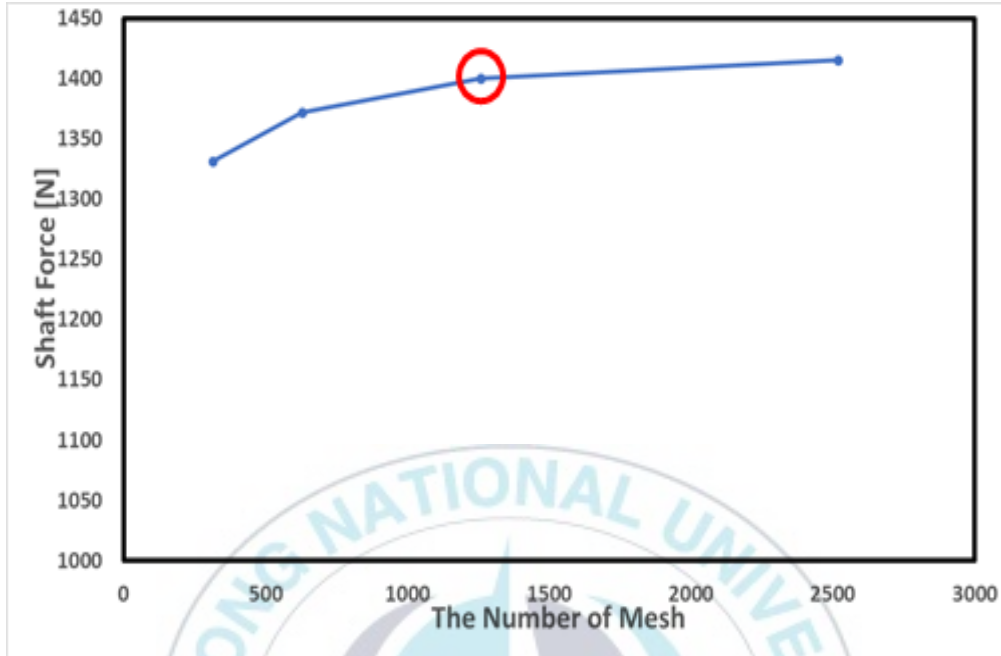


Figure 3.5: Analysis result according to the number of mesh of circumferential direction

3.1.2. Validation

The bearings to be analyzed in this study are generally oil-lubricated plain bearings that operate completely separated from the shaft and bearing surfaces by the lubricant film specified by the KS standard. For comparison with experimental data, the detailed dimensions of reference was made to Dhande and Pande [32].

Figure 3.6 shows the comparison of experimental and numerical results according to the rotational speed of the shaft. Figure 3.7 shows the comparison of experimental and numerical results according to the eccentricity. As a result of numerical analysis, when the rotation speed was changed, the error rate

tended to decrease as the rotation speed increased, and when the calculation was performed while increasing the eccentricity, the error rate decreased as the eccentricity increased.

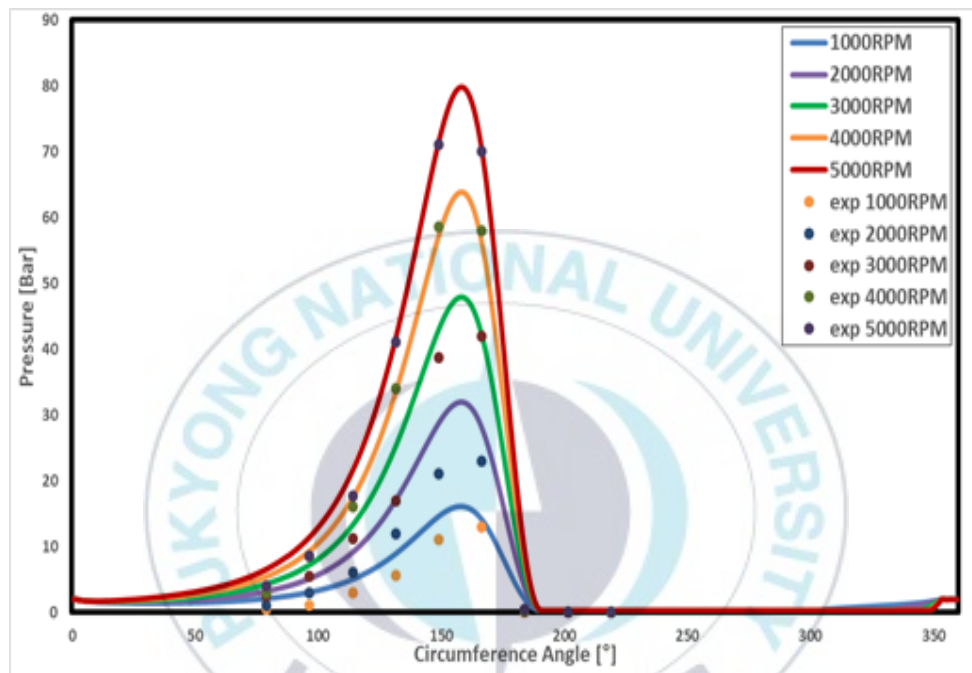


Figure 3.6: Comparison of experimental and numerical analysis results according to the rotational speed of the shaft

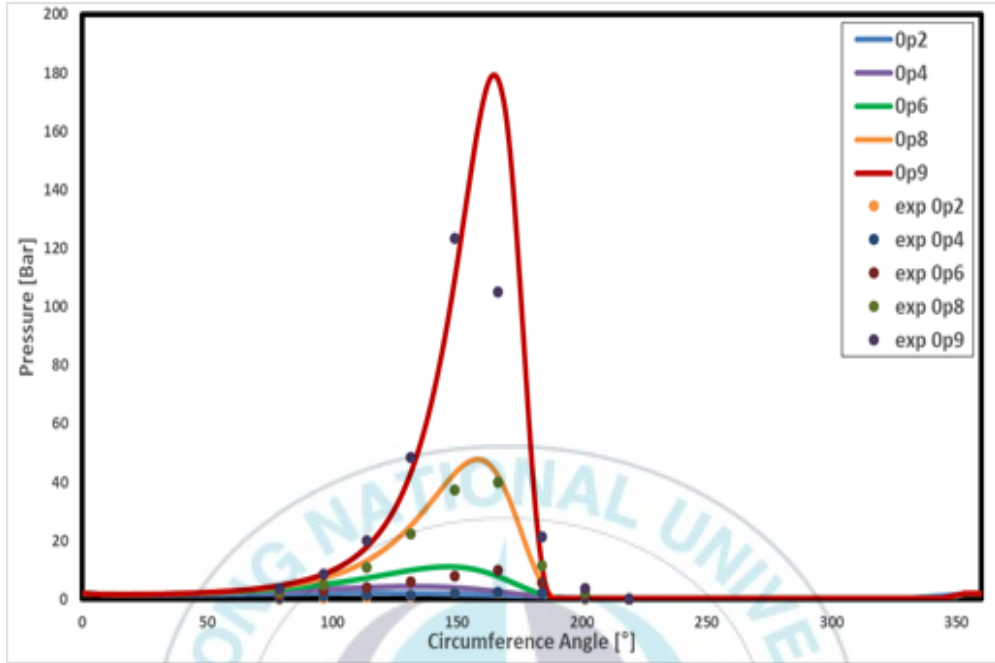


Figure 3.7: Comparison of experimental and numerical analysis results according to the eccentricity

3.2. Computational flow analysis according to viscosity change

When the bearing is lubricated, the efficiency of the bearing is related with the viscosity of the lubricant. Since the viscosity of the fluid is dominant in temperature, it is necessary to maintain the temperature by providing a suitable lubricant during operation. Viscosity can be expressed by equations for temperature and pressure as [33], [34].

$$\mu = \alpha e^{\frac{b}{T}} \quad (3.1)$$

Here,

$$b = \frac{\ln\mu_{40} - \ln\mu_{100}}{\frac{1}{T_{40}} - \frac{1}{T_{100}}} = 130.79 \quad (3.2)$$

Where, μ_T = Viscosity at temperature T .

$$\ln\alpha = \ln\mu_{40} - \frac{b}{T_{40}} \quad (3.3)$$

In μ_{40} , 40 is the size of the variable of the temperature in °C. When $\alpha = 1.706$ and $b = 130.79$, the viscosity according to temperature can be determined for the lubricant Turbine oil 30 (TP-30). Table 3.2 shows the properties of the Turbine oil 30 used in this study. Figure 3.8 shows the viscosity change of lubricant (TP-30) with temperature by Andrade equation. From the figure, it can be seen that as the temperature increases, the viscosity of the lubricant decreases.

Table 3.2: Properties of Turbine oil 30

Turbine Oil 30(TP-30)	
Density (15°C)	880 [kg/m^3]
Pour Point	-15 [°C]
Flash Point	235 [°C]
Viscosity (40°C, 100°C)	51, 7.17 [mm^2/s]
VI (Viscosity Index)	97

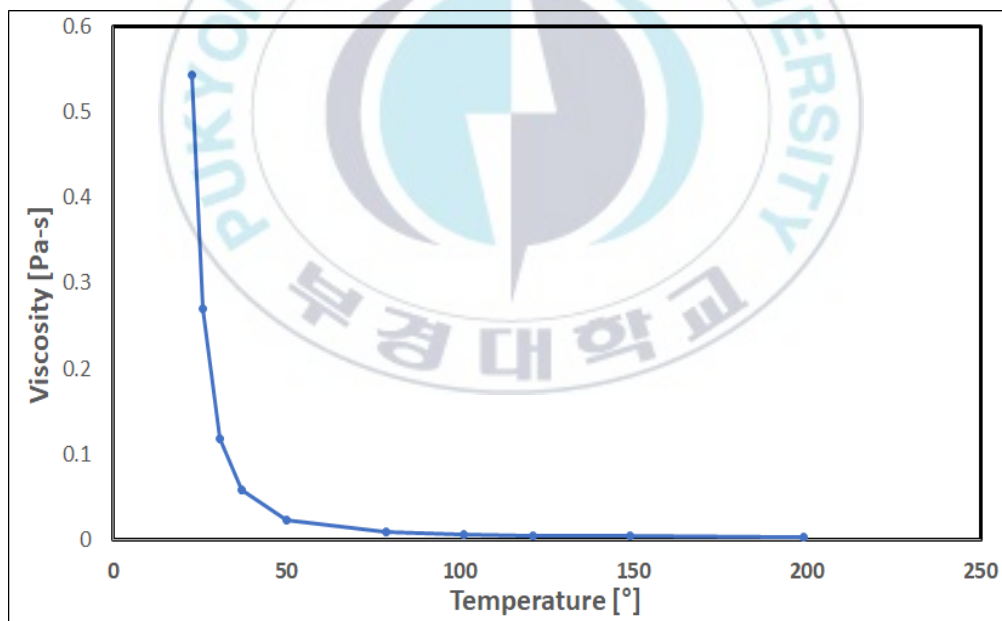


Figure 3.8: Viscosity change of lubricant (TP-30) with temperature by Andrade Equation

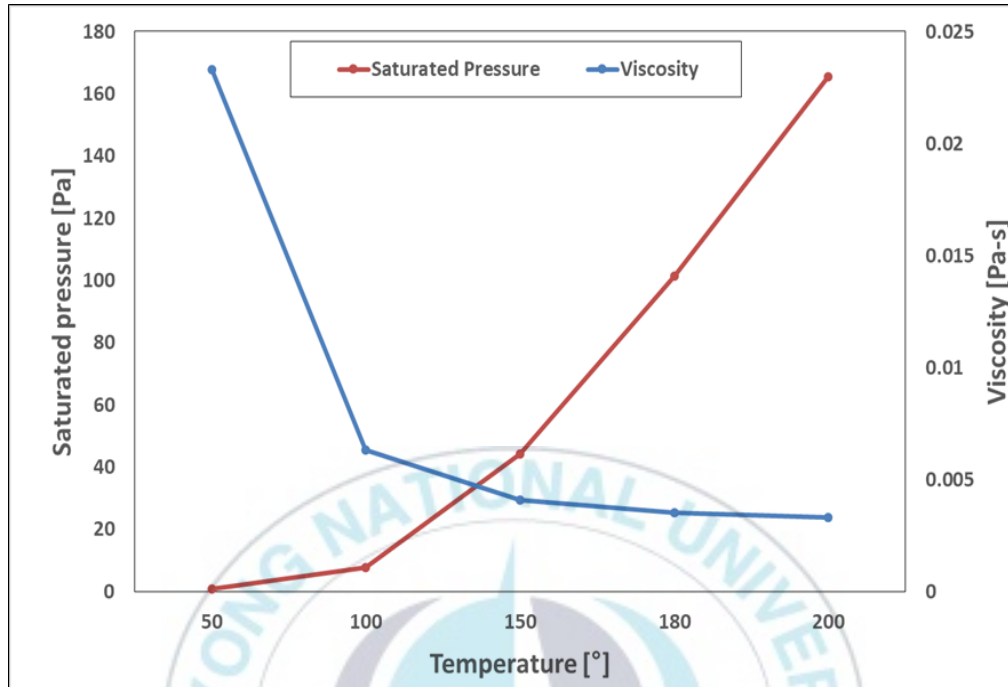


Figure 3.9: Variation of saturated vapor pressure with temperature

Not only does the viscosity change with temperature, but also the saturated vapor pressure of the lubricant changes, which affects the cavitation caused by the rapidly descending pressure after the eccentric. The saturated vapor pressure data according to temperature can be obtained through experiments from [20]. Figure 3.9 shows the variation of saturated vapor pressure with temperature. From the figure it can be seen that as the temperature increases, the saturated pressure increases and the viscosity decreases. The lubricant property values of saturated pressure and viscosity are used in the numerical calculations.

3.2.1. Flow field analysis

3.2.1.1. Pressure field

The bearing operating conditions and the degree of cooling varies from a minimum 80°C to a maximum 150°C. The lubricant Turbine oil 30 (TP-30) used in this analysis has a pour point of -15°C and a flash point of 235°C . Hence, the analysis was carried out with an assumption of extreme conditions from 50°C to 200°C . Also, a Revolutions Per Minute (RPM) of 3000 is used as fixed RPM. The eccentricity varies depending on the degree to which the bearing load is subjected. Hence, three different eccentricities of 0.6, 0.8 and 0.9 are used.

Figure 3.10 shows the pressure field with respect to temperature change at 3000 RPM for an eccentricity of 0.6. From the figure, it can be seen that as the temperature increases from 50°C to 200°C , the viscosity and pressure decreases. Similarly, Figures 3.11 and 3.12 shows the pressure field with respect to temperature change at 3000 RPM for eccentricities of 0.8 and 0.9 respectively. From these figures, it can be seen that as the temperature increases from 50°C to 200°C , the viscosity and pressure decreases similar to figure 3.10. As a result of analyzing eccentricities 0.6, 0.8, and 0.9, it was confirmed that the pressure decreases because the viscosity decreases as the temperature increases. As the temperature decreased, the viscosity increased in the form of a log function. From the figures, it was confirmed that the pressure also changed in response to the rate of viscosity change.

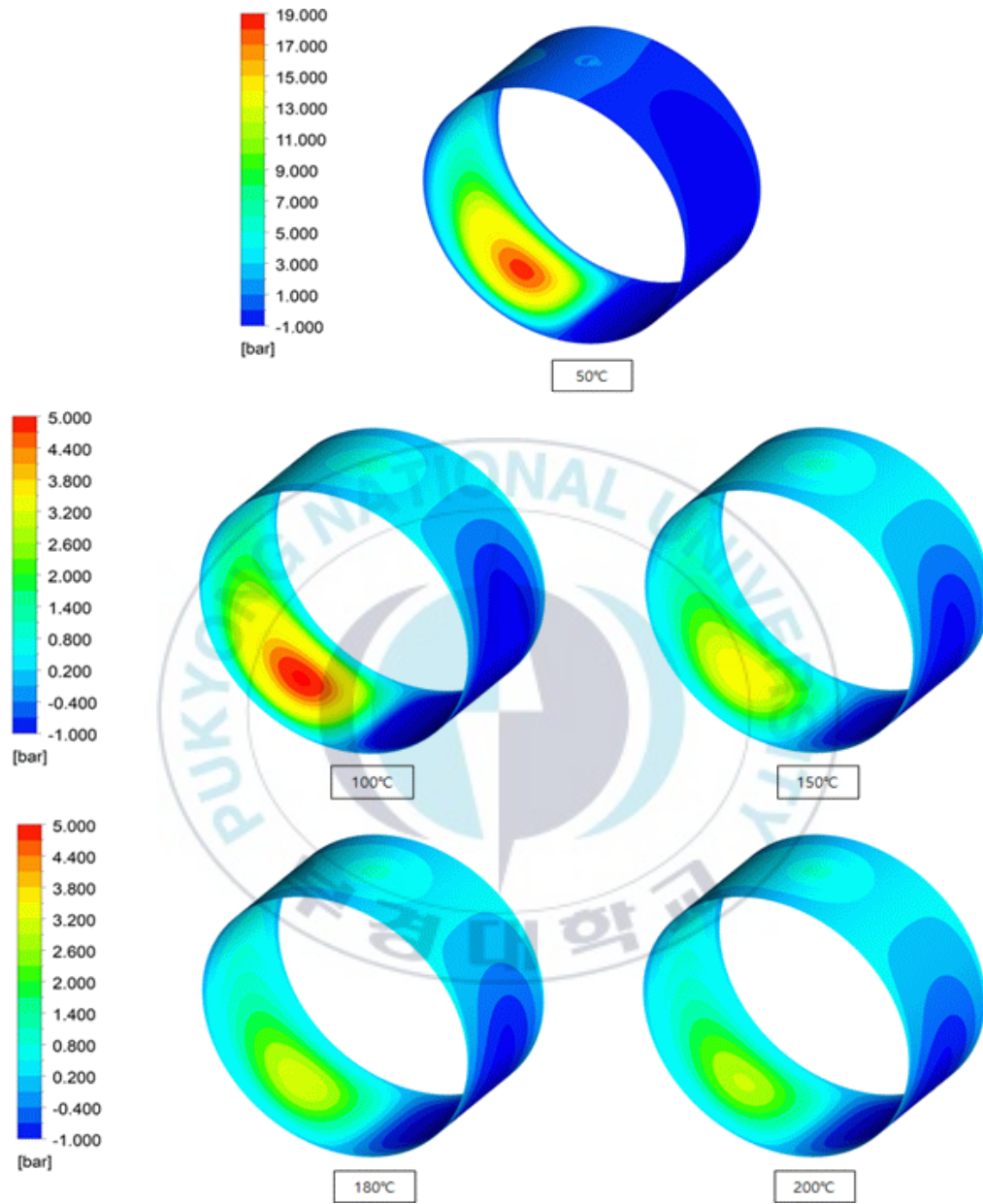


Figure 3.10: Pressure field according to temperature change at 3000RPM for eccentricity is 0.6

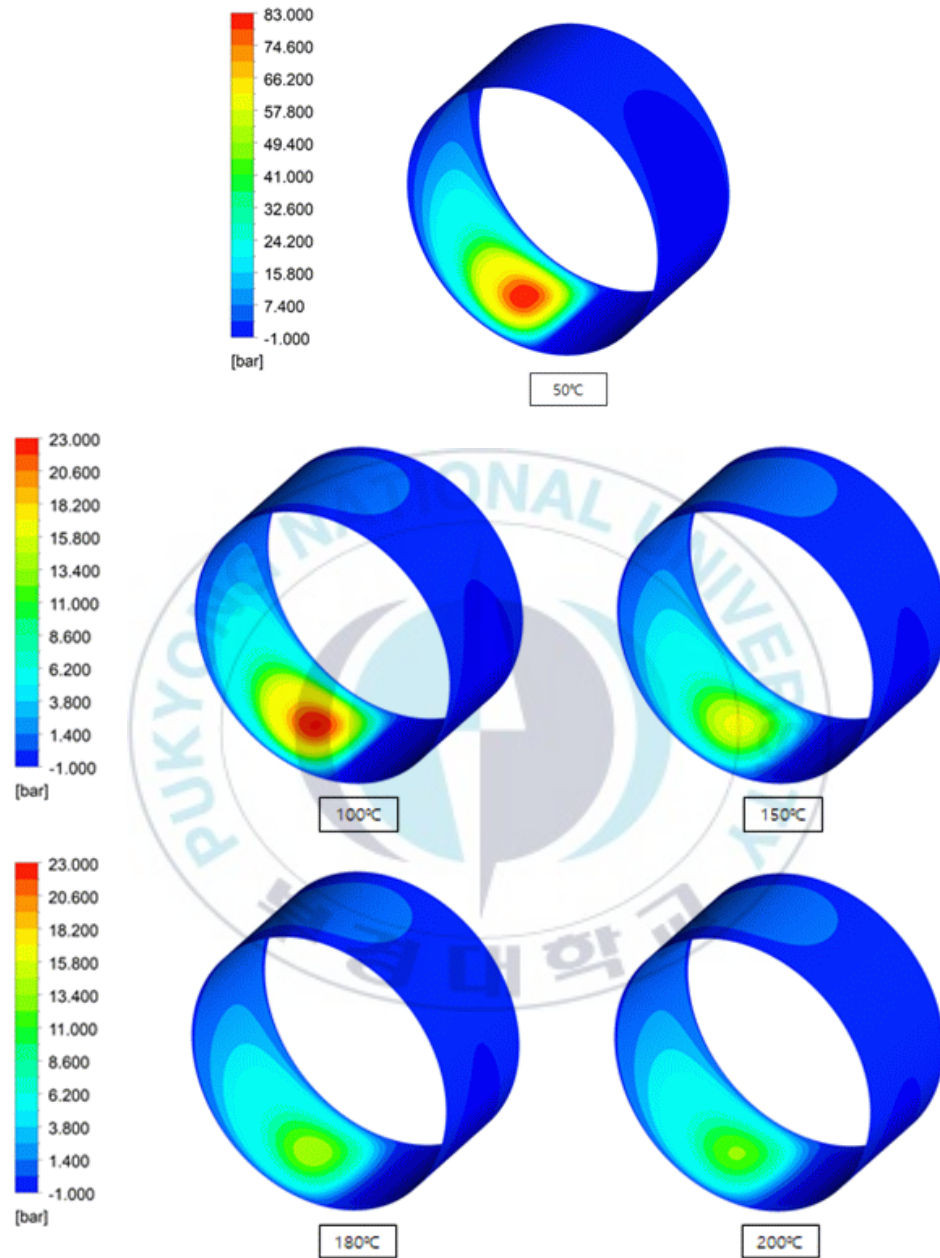


Figure 3.11: Pressure field according to temperature change at 3000RPM for eccentricity is 0.8

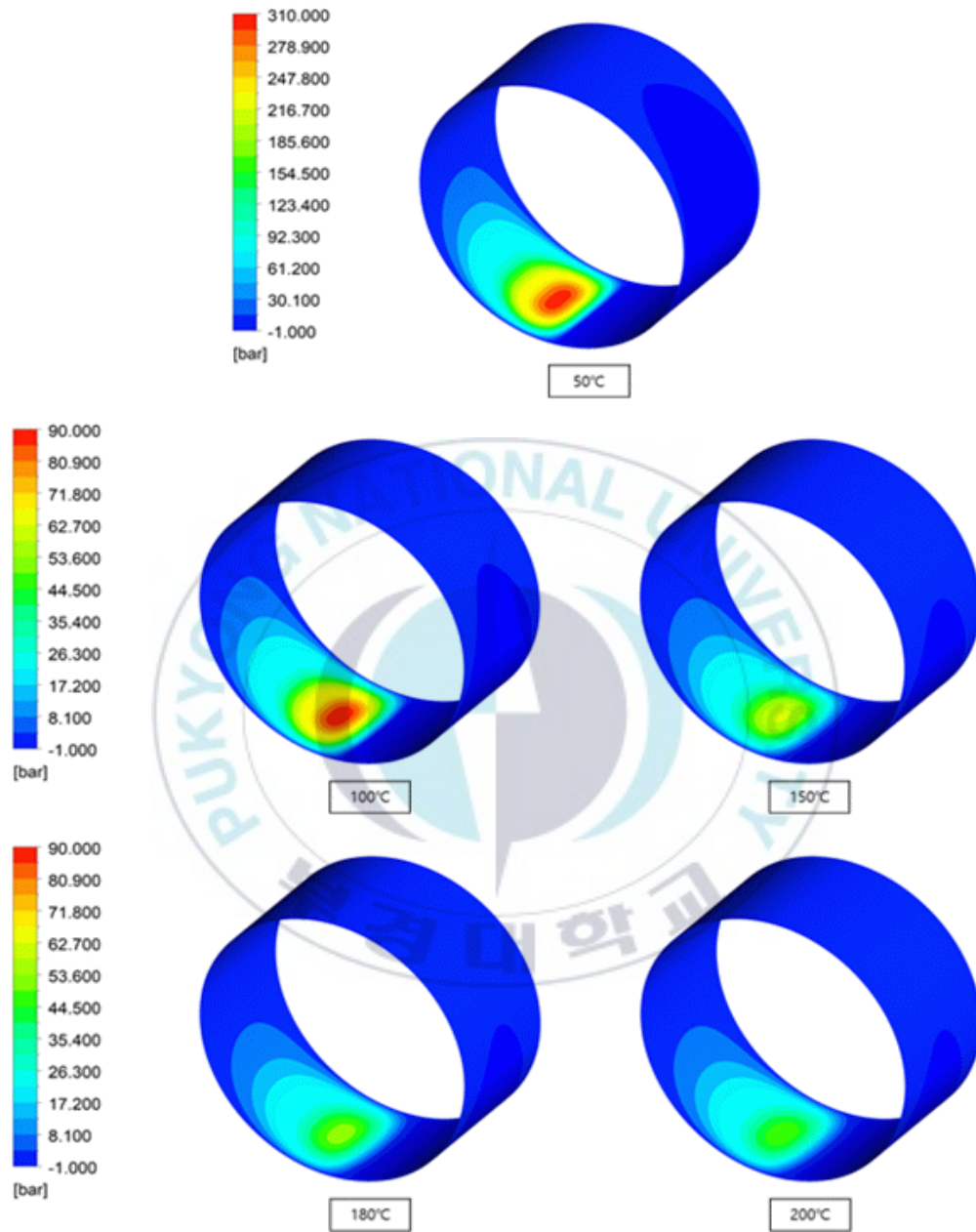


Figure 3.12: Pressure field according to temperature change at 3000RPM for eccentricity is 0.9

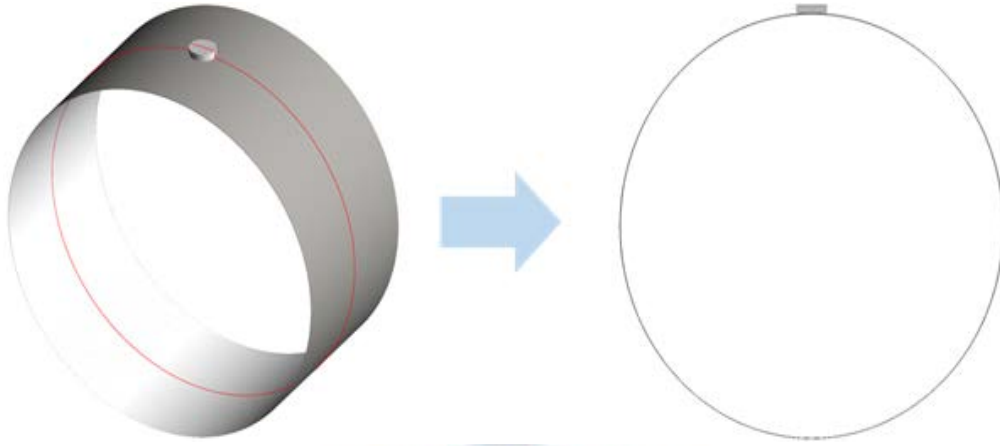


Figure 3.13: Plane view projection in the circumferential direction of the bearing

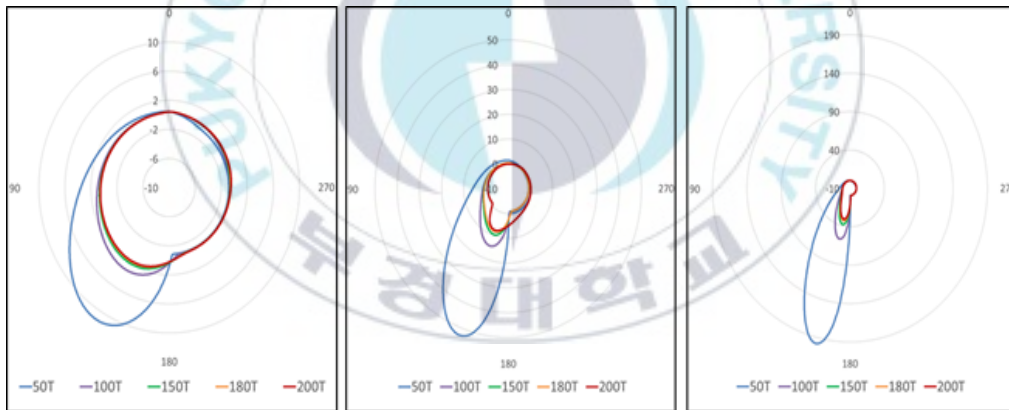


Figure 3.14: Circumferential pressure data applied to the bearing part

Figure 3.13 shows the plane view projection in the circumferential direction of the bearing. The figure shows the center line of the shaft – that is set to rotate in the counter-clockwise direction – and the corresponding circumferential pressure data applied to the bearing part is plotted for

temperatures varying from 50°C to 200°C, as shown in Figure 3.14. From figure 3.14, we can see that as the temperature increases, the circumferential pressure distribution decreases for eccentricities of 0.6, 0.8 and 0.9 respectively. Also, it can be seen that the numerical pressure distribution profile matches the theoretical pressure distribution profile as shown in figure 2.3.

3.2.1.2. Volume fraction of gaseous lubricant

Figure 3.15 shows the plane view projection along the width direction of the bearing. The shaft is set to rotate in the counter-clockwise direction. Figure 3.16, 3.17 and 3.18 shows the volume fraction of lubricant in the gaseous phase with respect to the plane projected in the width direction of the bearing – for a revolution of 3000 RPMs and temperature change from 50°C to 200°C – for eccentricities 0.6, 0.8 and 0.9 respectively. When the pressure drops sharply after the minimum lubricating thickness and falls below the vapor pressure, a cavitation phenomenon occurs in which the liquid lubricant changes to a gaseous state. This not only affects the lubrication performance of the bearing, but also the permissible load. When cavitation occurs, the maximum pressure is reduced by bubbles of oil vapor, but in severe cases, the bubbles may impact the bearing surface and cause noise, vibration and wear. As the bearing temperature increases and the eccentricity increases, the volume fraction increases as shown in figure 3.19.

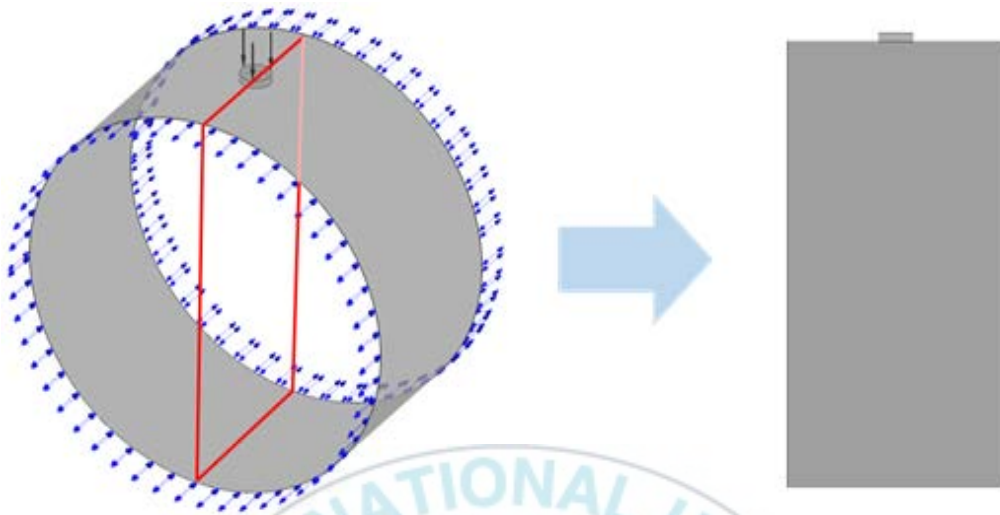


Figure 3.15: Plane view projection in the width direction of the bearing

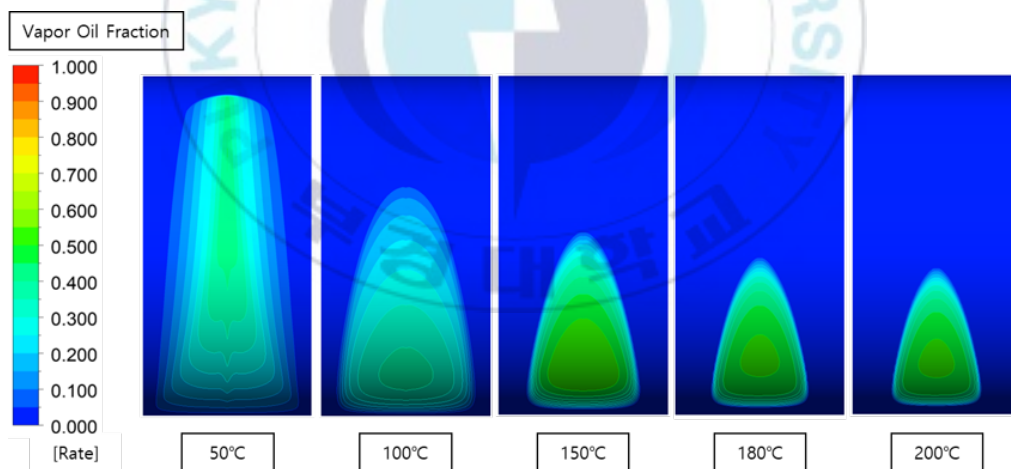


Figure 3.16: Volume fraction of the gaseous lubricant in the width direction of the bearing according to the temperature at 3000RPM when the eccentricity is 0.6

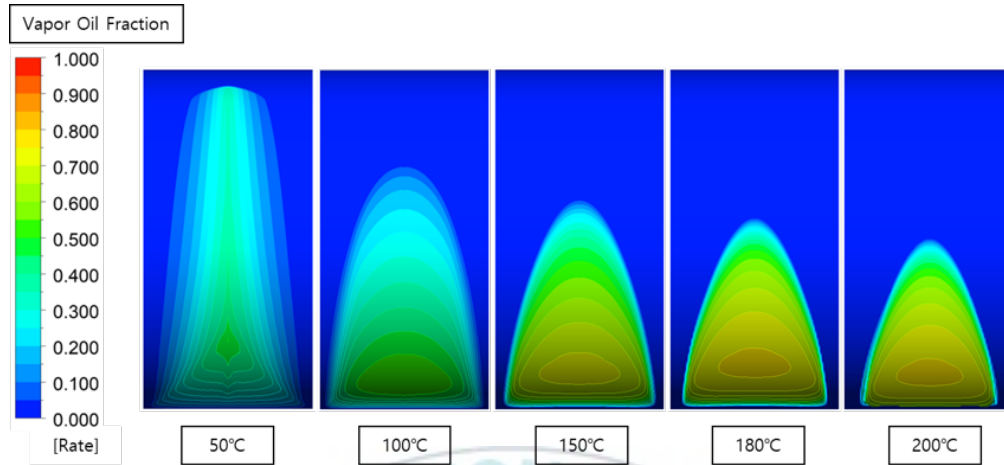


Figure 3.17: Volume fraction of the gaseous lubricant in the width direction of the bearing according to the temperature at 3000 RPM when the eccentricity is 0.8

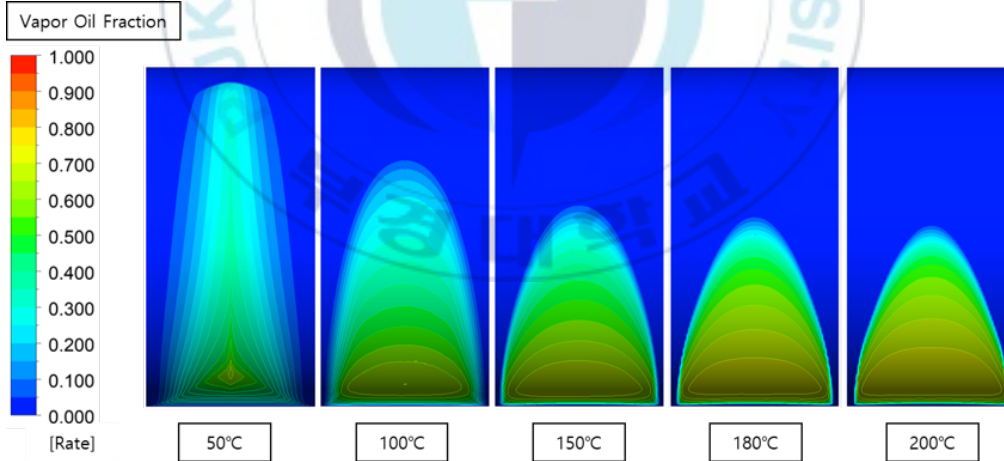


Figure 3.18: Volume fraction of the gaseous lubricant in the width direction of the bearing according to the temperature at 3000 RPM when the eccentricity is 0.9

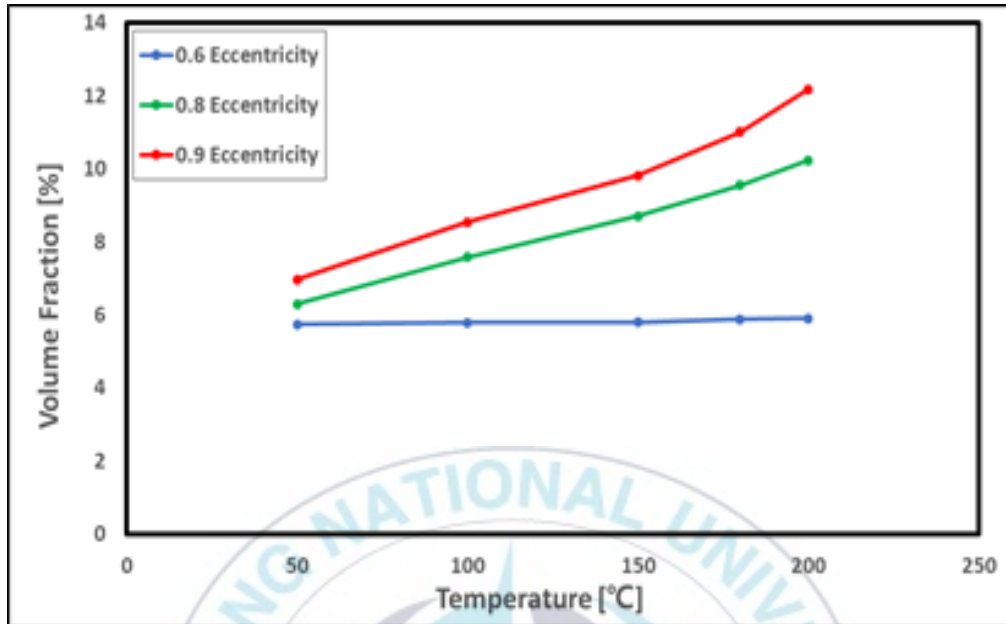


Figure 3.19: Volume fraction at the bearing surface with temperature

3.2.2. Comparison of force and attitude angle

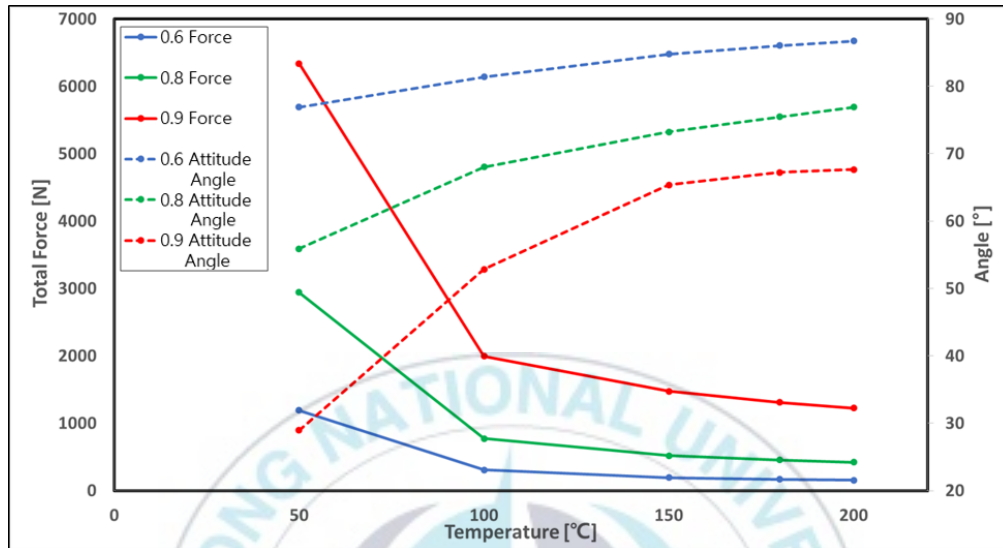


Figure 3.20: Force and attitude angle according to temperature

Figure 3.20 shows the force and attitude angle changes with respect to temperature. From the figure, it can be seen that as the temperature of the lubricant increases the pressure applied to the bearing surface decreases and thus the reaction force applied to the shaft decreases. As the magnitude of eccentricity and combined force changes, the part where the actual force acts changes, which is called attitude angle. As the temperature increases, the force applied to the shaft decreases and the attitude angle appears further than the minimum lubrication thickness.

3.3. Computational flow analysis based on rotational speed

3.3.1. Flow field analysis

3.3.1.1. Pressure field

The greater the load applied to the bearing, the higher the rotational speed required. The bearing operating conditions and the degree of rotation speed varies from a minimum 1000 RPM to a maximum 5000 RPM. The analysis was carried out with an assumption of extreme conditions for 50°C. The eccentricity varies depending on the degree to which the bearing load is subjected. Hence, three different eccentricities of 0.6, 0.8 and 0.9 are used.

Figure 3.21 shows the pressure field with respect to rotating speed changes of RPMs 1000 to 5000 at 50°C for an eccentricity of 0.6. From the figure, it can be seen that as the rotating speed increases from 1000 RPM to 5000 RPM, the pressure increases. Similarly, Figures 3.22 and 3.23 shows the pressure field with respect to rotating speed changes of RPMs 1000 to 5000 at 50°C for eccentricities of 0.8 and 0.9 respectively. From these figures, it can be seen that as the rotating speed increases from 1000 to 5000 RPMs, the pressure increases similar to figure 3.21. As a result of analyzing eccentricities 0.6, 0.8, and 0.9, it was confirmed that the pressure increases because the rotating speed increases. Also, as the rotating speed increased, the pressure increased in the form of a linear function. From the figures, it was confirmed that the pressure also changed in response to the rate of rotating speed change.

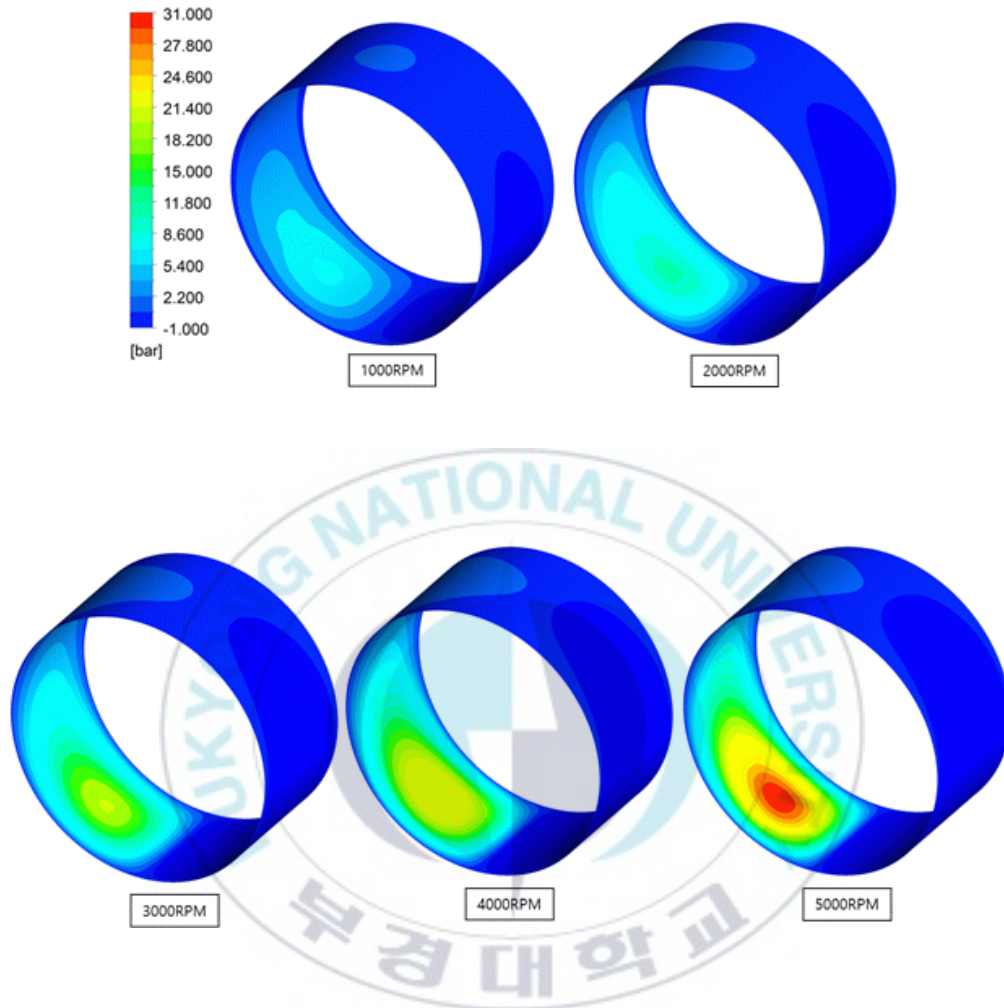


Figure 3.21: Pressure field according to rotating speed changes at 50°C for eccentricity is 0.6

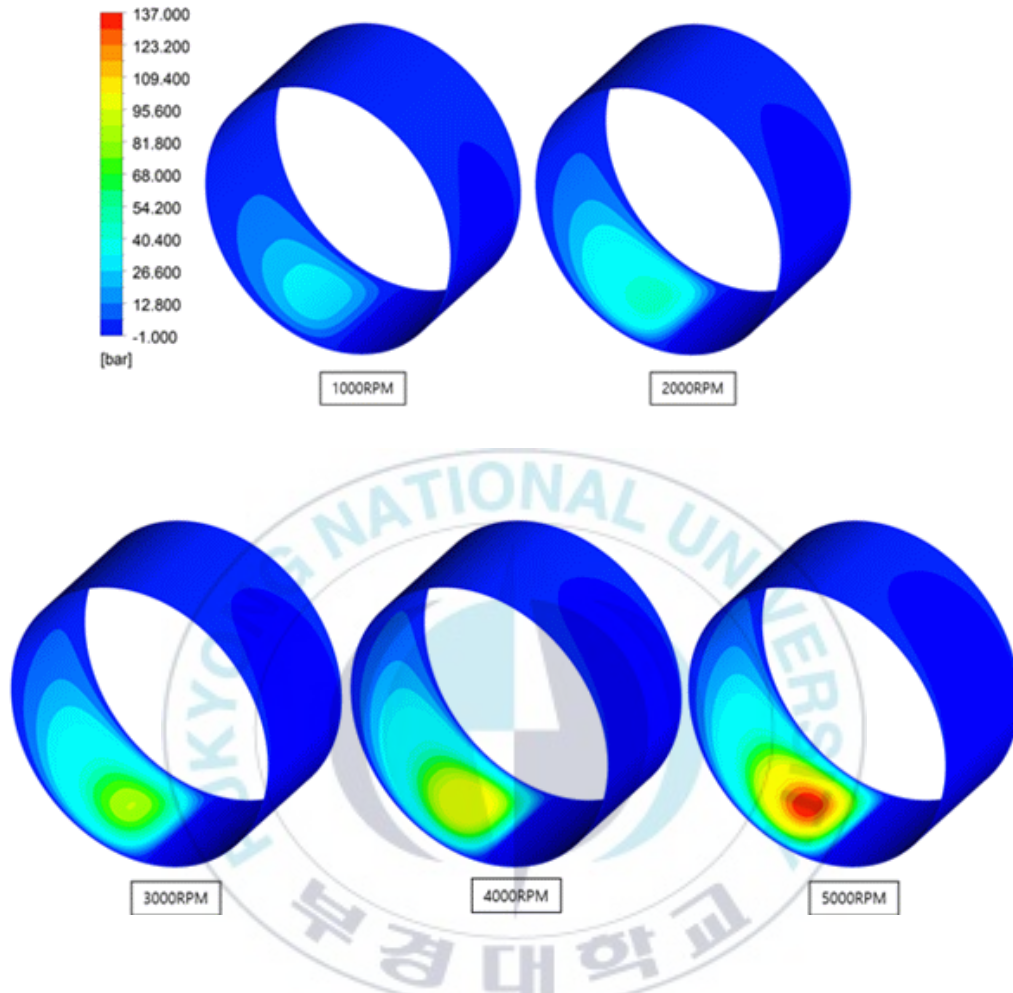


Figure 3.22: Pressure field according to rotating speed changes at 50°C for eccentricity is 0.8

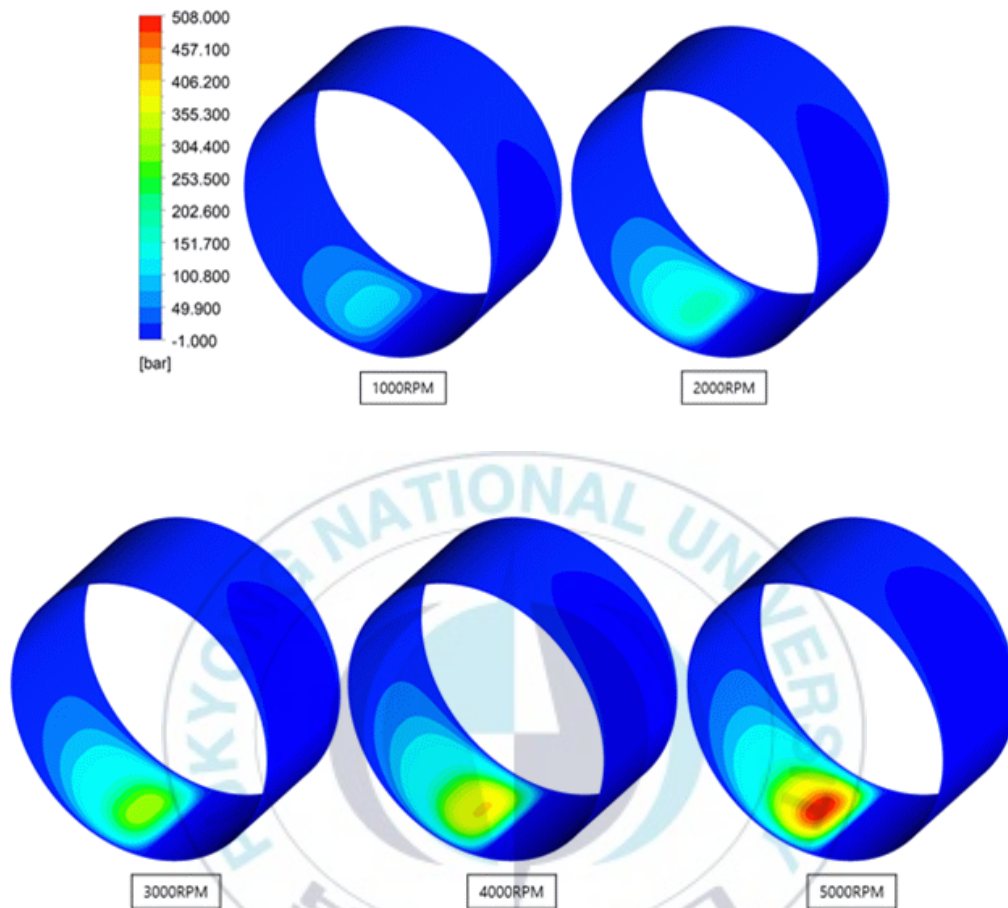


Figure 3.23: Pressure field according to rotating speed changes at 50°C for eccentricity is 0.9

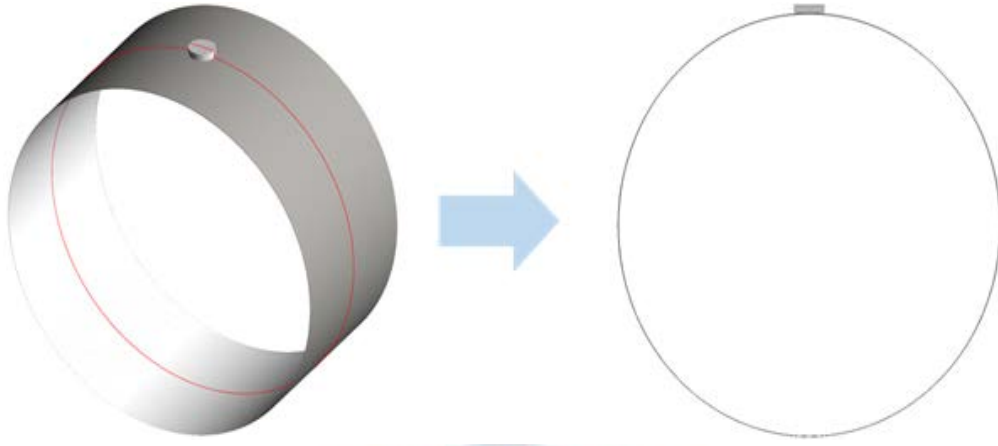


Figure 3.24: Plane view when projecting in the circumferential direction of the bearing

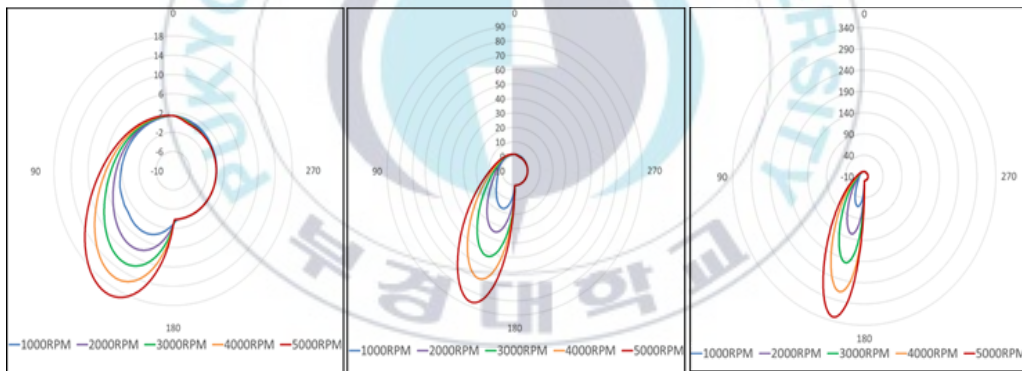


Figure 3.25: Circumferential pressure data applied to the bearing

Figure 3.24 shows the plane view projection in the circumferential direction of the bearing. The figure shows the center line of the shaft – that is set to rotate in the counter-clockwise direction – and the corresponding circumferential pressure data applied to the bearing part is plotted for rotating

speeds varying from 1000 to 5000 RPMs as shown in Figure 3.25. From figure 3.25, we can see that as the rotating speed increases, the circumferential pressure distribution increases for eccentricities of 0.6, 0.8 and 0.9 respectively. Also, it can be seen that the numerical pressure distribution profile matches the theoretical pressure distribution profile as shown in figure 2.3.

3.3.1.2. Volume fraction of gaseous lubricant

Figure 3.26 shows the plane view projection along the width direction of the bearing. The shaft is set to rotate in the counter-clockwise direction. Figure 3.27, 3.28 and 3.29 shows the volume fraction of lubricant in the gaseous phase with respect to the plane projected in the width direction of the bearing – for a revolution of 1000 to 5000 RPMs and rotating speed changes of 50°C – for eccentricities 0.6, 0.8 and 0.9 respectively. When the pressure drops sharply after the minimum lubricating thickness and falls below the vapor pressure, a cavitation phenomenon occurs in which the liquid lubricant changes to a gaseous state. This not only affects the lubrication performance of the bearing, but also the permissible load. When cavitation occurs, the maximum pressure is reduced by bubbles of oil vapor, but in severe cases, the bubbles may impact the bearing surface and cause noise, vibration and wear. As the bearing rotating speed increases and the eccentricity increases, the volume fraction increases in the form of a linear function as shown in figure 3.30.

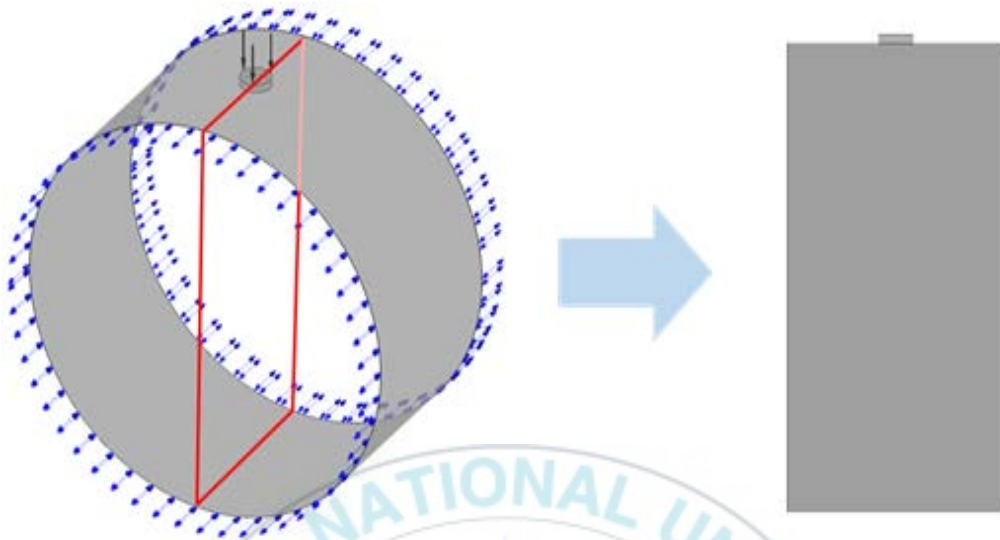


Figure 3.26: Plane view when projection in the width direction of the bearing

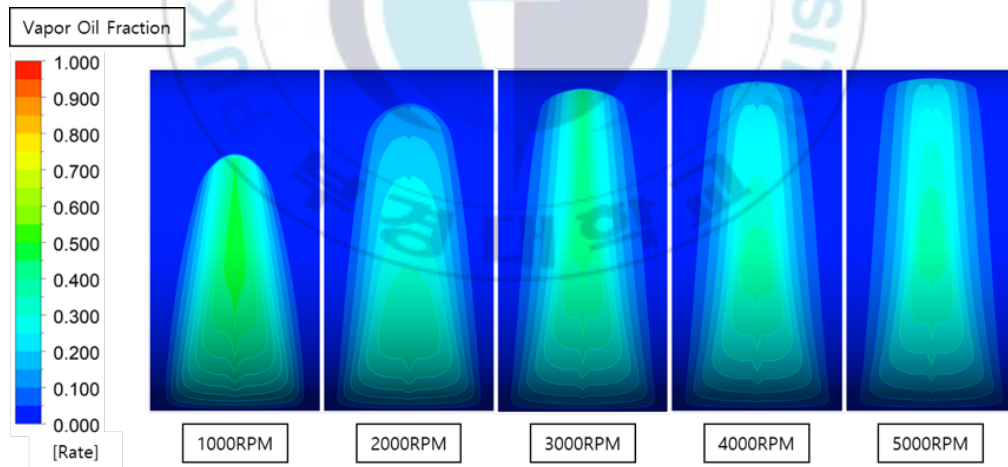


Figure 3.27: Volume fraction of the gaseous lubricant in the width direction of the bearing according to the rotating speed at 50°C when the eccentricity is 0.6

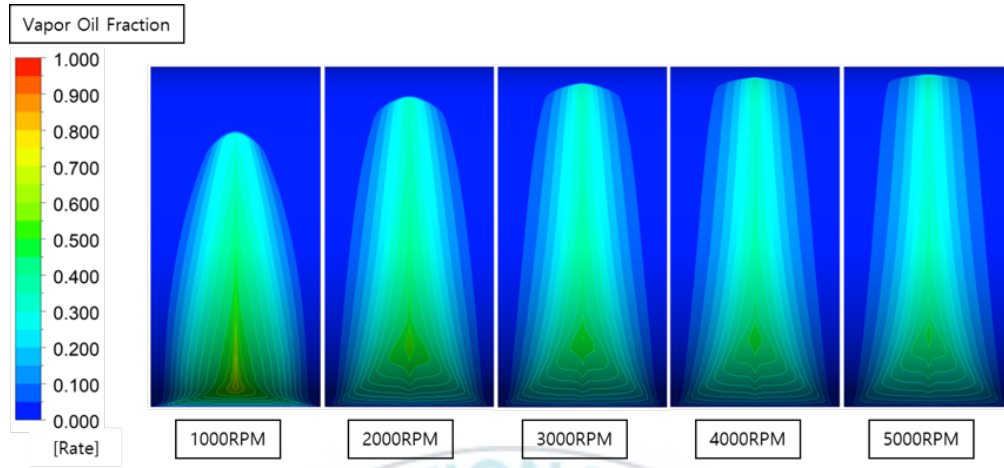


Figure 3.28: Volume fraction of the gaseous lubricant in the width direction of the bearing according to the rotating speed at 50°C when the eccentricity is 0.8

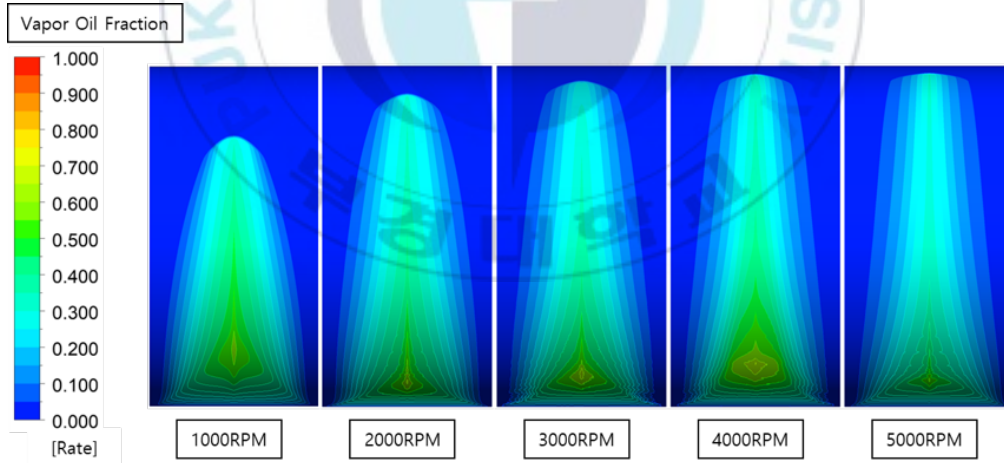


Figure 3.29: Volume fraction of the gaseous lubricant in the width direction of the bearing according to the rotating speed at 50°C when the eccentricity is 0.9

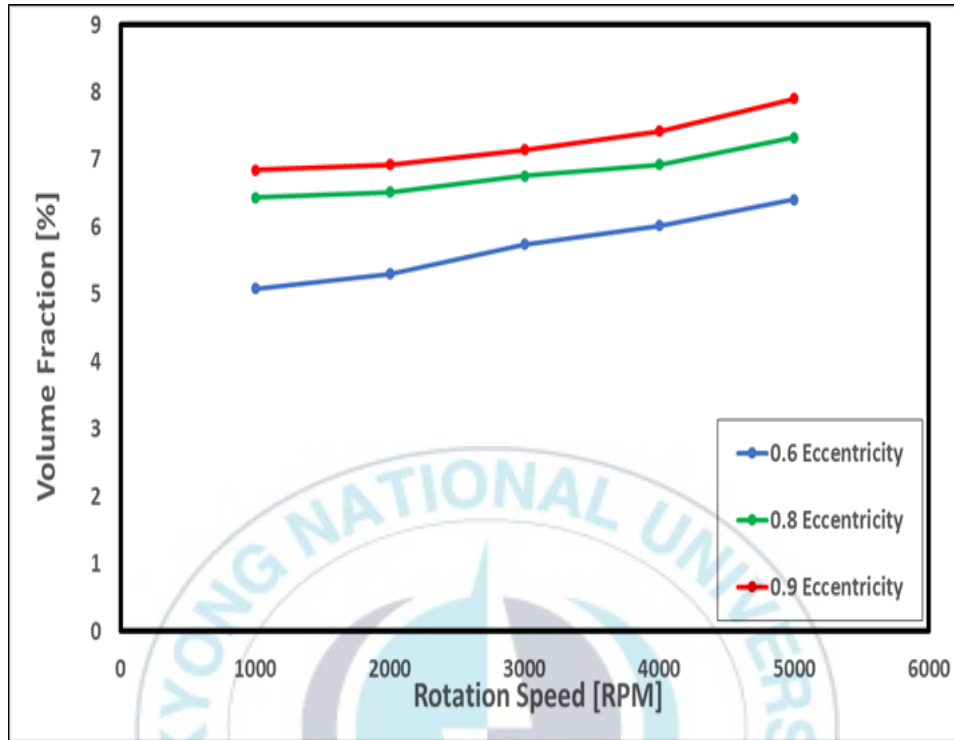


Figure 3.30: Volume fraction at the bearing surface with temperature

3.3.2. Comparison of force and attitude angle

Figure 3.31 shows the force and attitude angle changes with respect to rotation speed. From the figure, it can be seen that as the rotating speed of the shaft increases the pressure applied to the bearing surface increases and thus the reaction force applied to the shaft increases. As the magnitude of eccentricity and combined force changes, the part where the actual force acts changes, which is called attitude angle. As the rotating speed increases, the force applied to the shaft increases and the attitude angle appears closer than the minimum lubrication thickness.

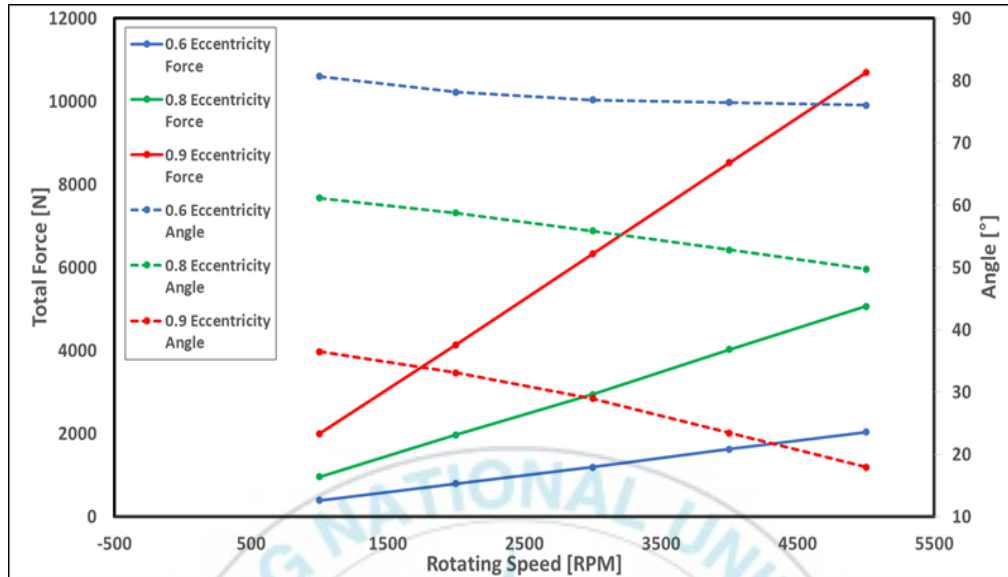


Figure 3.31: Force and attitude angle according to rotation speed

3.4. Introduction of dimple structure to investigate bearing performance

When the bearing is in operation, it is difficult to maintain complete fluid lubrication and also the boundary lubrication occurs frequently. Moreover, when the bearing does not have sufficient supporting capacity due to static load, dynamic load, boundary lubrication conditions, etcetera, the area of the load bearing decreases and the amount of wear and tear increases, thus resulting in a decrease in life, increase in noise and vibration and shorter replacement cycles. In order to solve this problem, in this study, a lubricating structure – dimple – is proposed to reduce the friction pressure generated during bearing operation by changing the bearing shape.

3.4.1. Assessment of dimple effect

Figure 3.32 shows the schematic of the bearing flow field with simple dimple structure. In this study, the dimple structure was used in the circumferential direction as well as in the width direction with various diameter and spatial changes in order to make a parametric study. The performance of the bearing – with and without dimple structure – was evaluated numerically. Table 3.3 shows the dimple parameters used in this study. A total of 6 cases with various dimple diameters, width direction numbers, circumferential angles and circumferential numbers were used to evaluate the performance of the bearing with dimple structures.

Table 3.3: Dimple parameters

Case	Dimple diameter [mm]	Width direction number [pc]	Circumferential angle [°]	Circumferential number [pc]
1	2	7	10	18
2	1	7	10	18
3	2	5	10	18
4	2	7	20	9
5	2	7	10	4
6	1	7	10	4

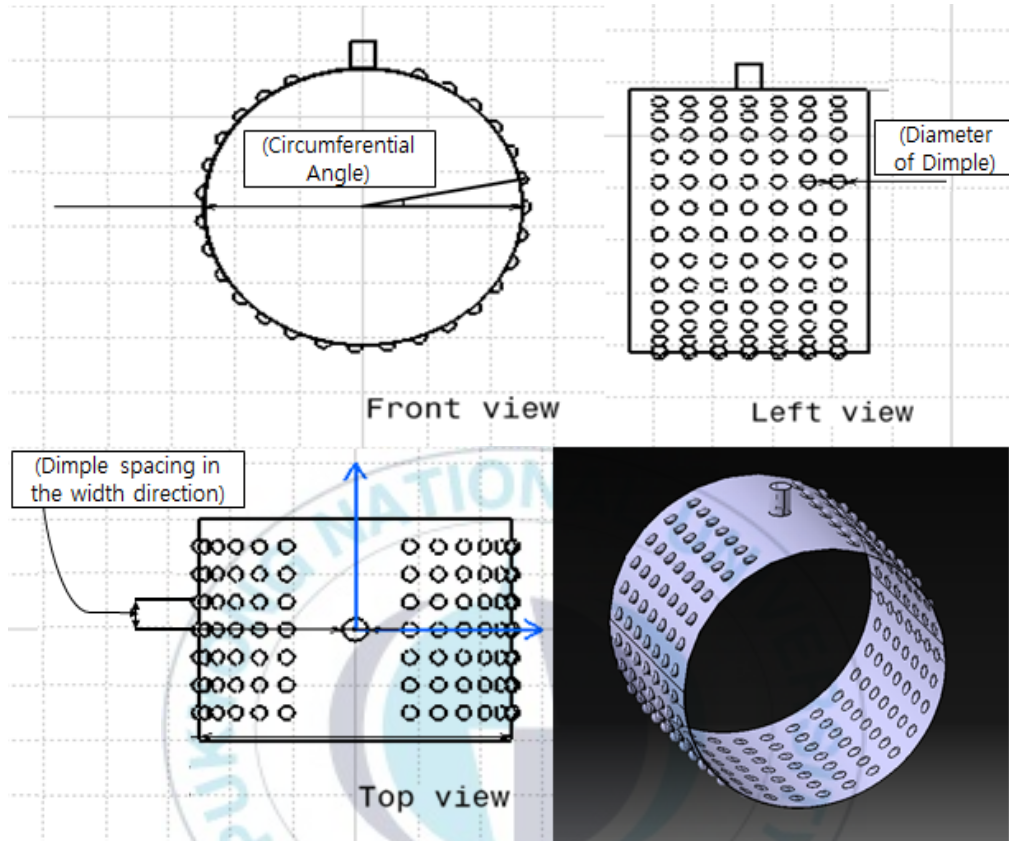


Figure 3.32: Schematic of the bearing flow field with simple dimple structure

Figure 3.33 shows the comparison of pressure field and volume fraction with and without dimple structure. From the numerical results, it was confirmed that the pressure applied to the bearing surface is reduced by 45% for the case of dimple structure than in a plain bearing. Also, it was confirmed that the force applied to the shaft decreased for the dimple structure. Moreover, the volume fraction of the gaseous lubricant decreased due to the reduction of the pressure drop, which could prevent the erosion caused by cavitation in advance. With the introduction of the dimple structure, the direct contact between the shaft and the

bearing that occurs during solid lubrication is reduced. The negative effect (reduction of the applied force) could be improved by changing the parameters of the dimple structure as discussed in Section 3.4.2.

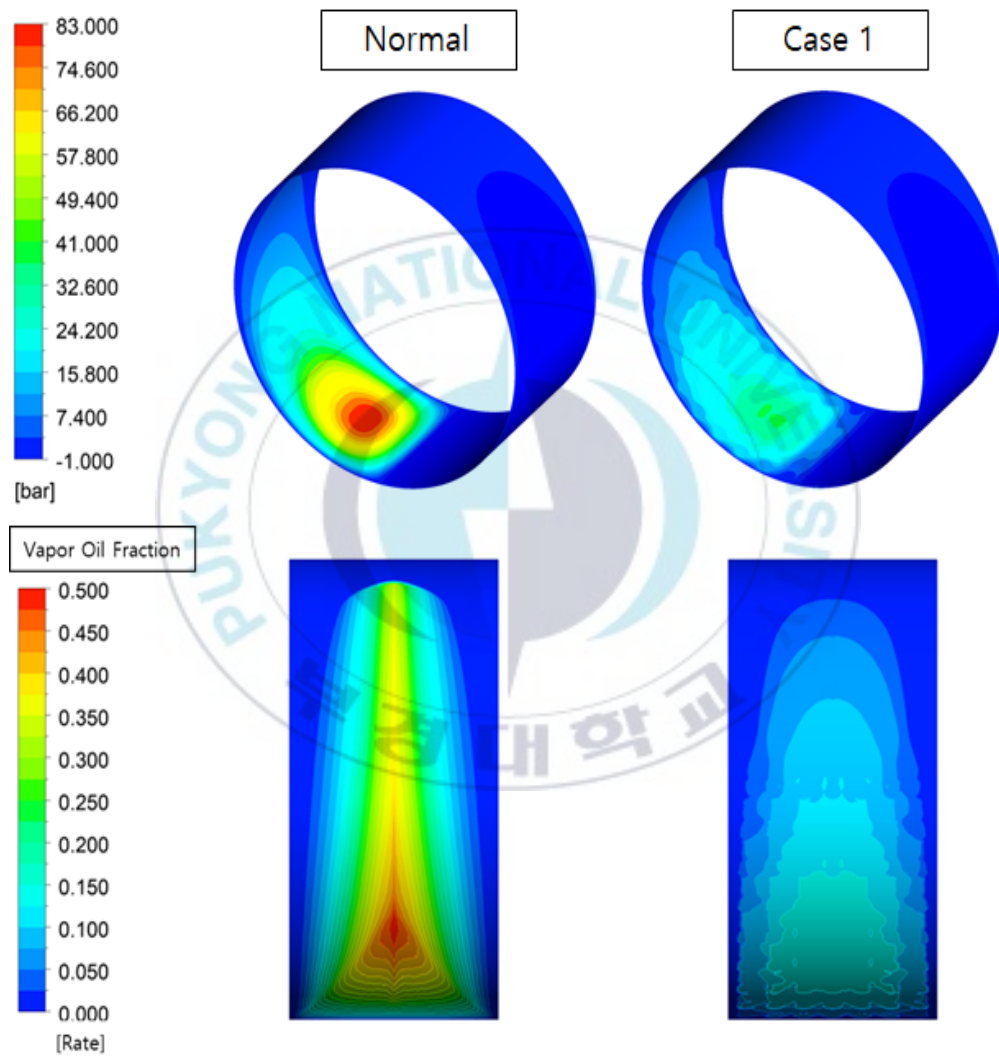


Figure 3.33: Comparison of pressure field and volume fraction with and without dimple structure

3.4.2. Effect of change of dimple parameters

In order to compare the effect of the dimple structure in the bearing, the bearing shape, the lubricant temperature at 50°C , the rotational speed of the shaft 3000 RPM, and the eccentricity 0.8 was fixed and the diameter and the spatial arrangement of the dimple were changed and analyzed.

Figure 3.34 shows the pressure field according to dimple parameter changes at 50°C , with a rotational speed of 3000 RPM for eccentricity of 0.8. From the figure, it can be seen that the pressure of Case 2 is higher when compared to other cases. Also, Case 1 registered the lowest pressure among the remaining cases. Figure 3.35 shows the volume fraction of the gaseous lubricant of the dimple bearing changes at 50°C , with a rotational speed of 3000 RPM for eccentricity of 0.8. From the figure, it can be seen that Case 6 has higher volume fraction whereas Case 5 has lower volume fraction.

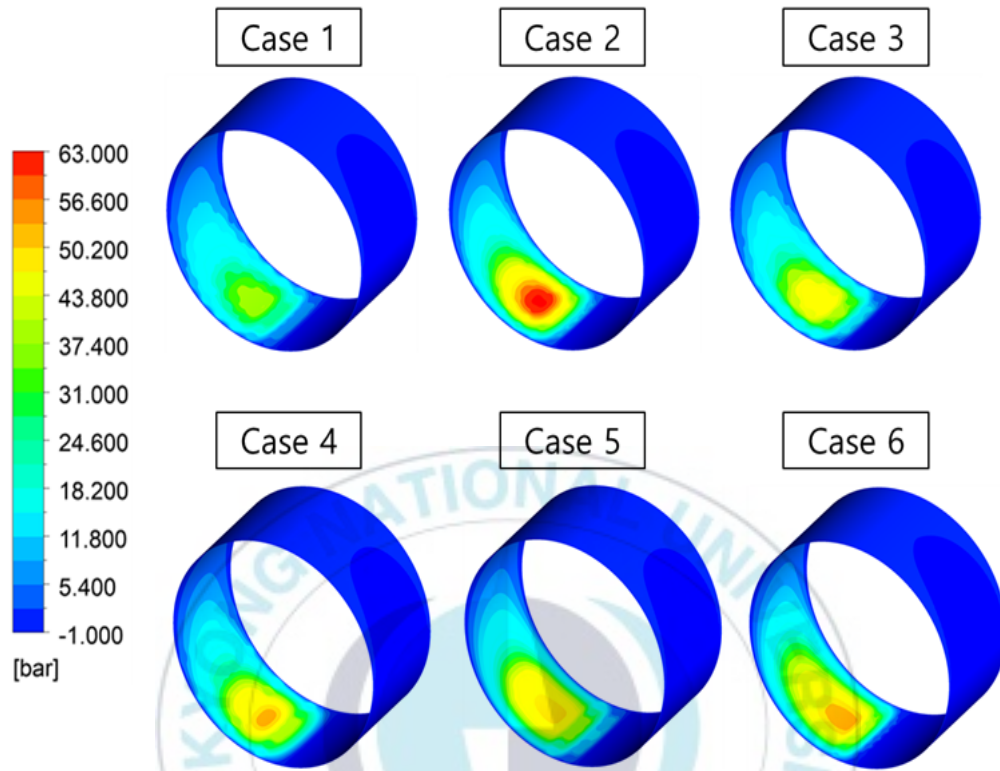


Figure 3.34: Pressure field according to dimple parameter changes at 50°C, 3000 RPM for eccentricity 0.8

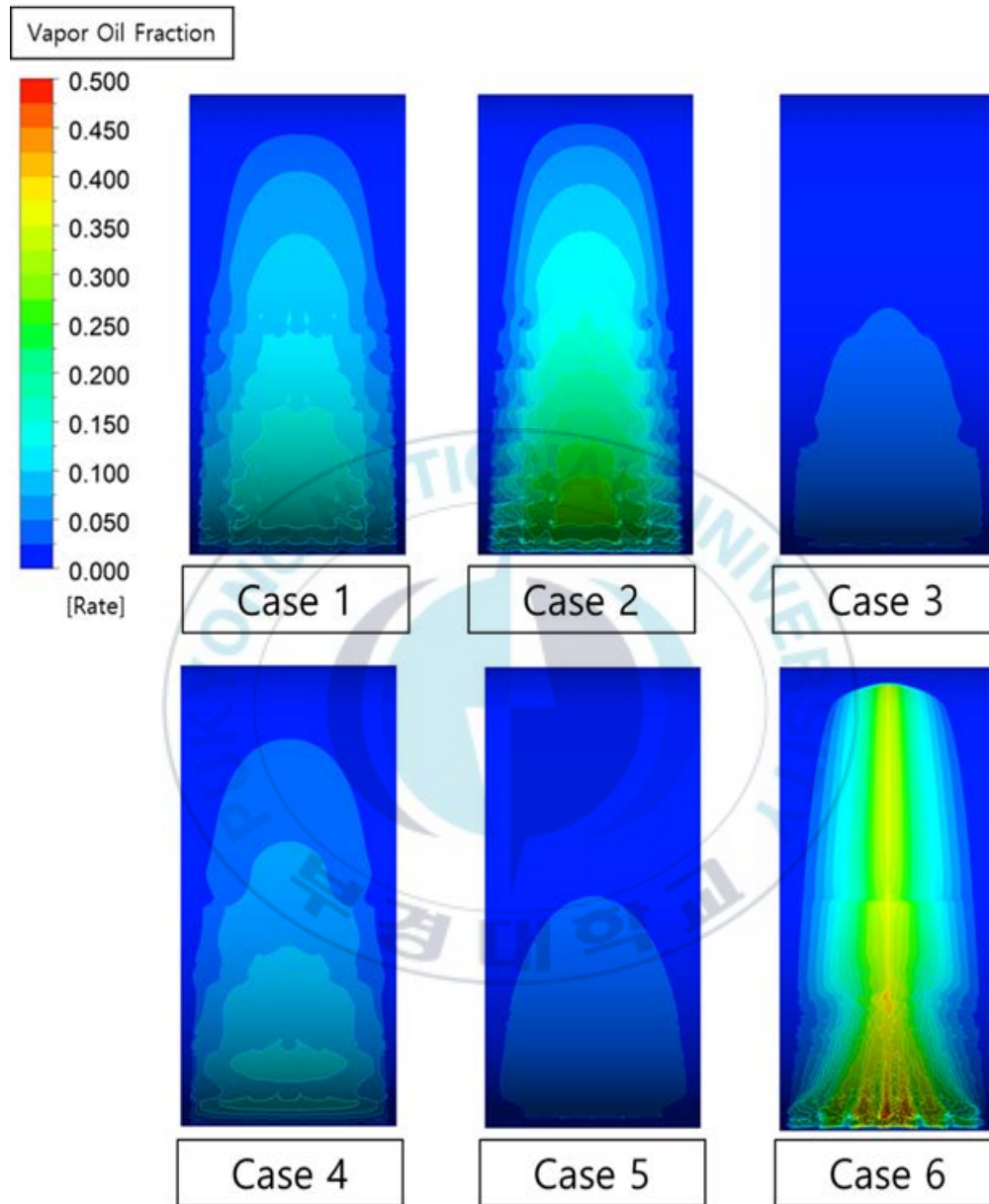


Figure 3.35: Volume fraction of the gaseous lubricant of the dimple parameter changes at 50°C, 3000 RPM for eccentricity 0.8

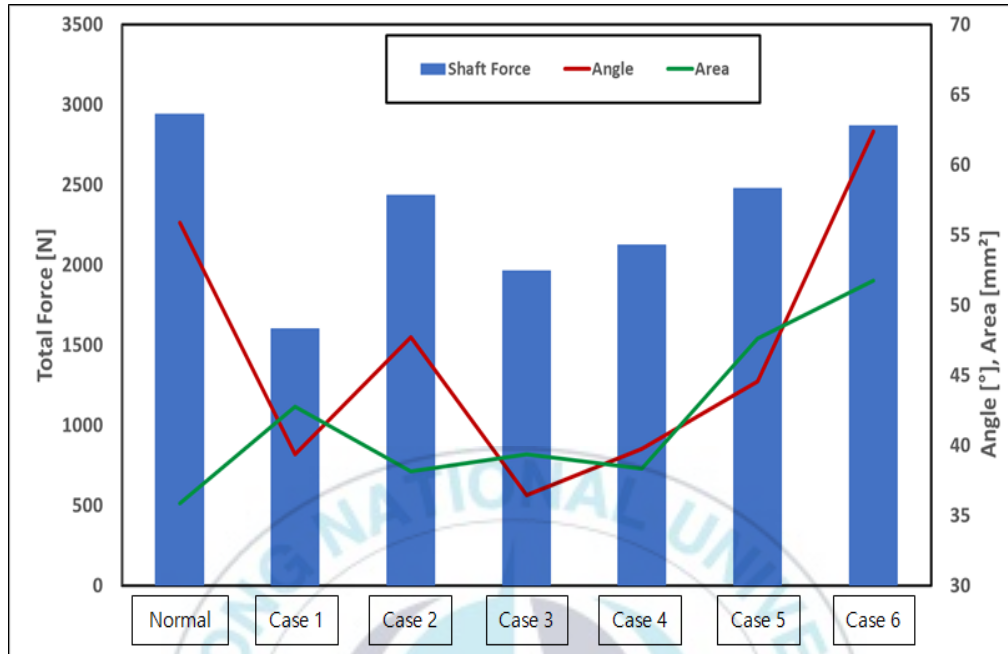


Figure 3.36: Force, attitude angle and average load area according to dimple structure pattern

Figure 3.36 shows the force, attitude angle and average load area of the dimple structure. The results show that as the shape of the dimple changes (Case 1, Case 2, ... , Case 6), the attitude angle tends to increase – with fluctuations – as the force applied to the shaft is increased (red line). When the dimple structure was used, the overall force applied to the shaft tend to decrease – when compared to the Normal case. When the diameter of Case 2 and circumferential space of Case 5 were changed, they found to be have higher forces than Cases 1, 3, and 4. When the diameter and circumferential space of Case 6 were changed, the force of Case 6 was found to be almost equal to the force of the Normal case. Case 6 also showed the highest efficiency (green line) when

considering the total force of the shaft taking into account the pressure and allowable load on the bearing. As a result of this analysis, it can be seen that changes in the shape and arrangement of the dimple have a great influence on the performance of the bearing and more reasonable shapes can be found through more parametric studies.



4. Conclusions

The lubrication of the bearing is a complex mechanism in which the change in temperature, change in eccentricity and the change in the force applied to the shaft are mutually dependent. In this study, the characteristics of journal bearing are investigated through a detailed three-dimensional flow analysis of the bearing and the performance is evaluated by means of CFD techniques. Also, a simple dimple structure and its performance improvement is discussed. As a result of the analysis, the following conclusions are drawn.

1. When the temperature increases, the viscosity of the lubricant decreases in the form of a log function. Hence, it is important to manage the temperature of the lubricant.
2. When the temperature increases, the viscosity of the lubricant and the internal pressure of the bearing decreases. Since the vapor pressure also increases with increasing temperature, it was confirmed that the volume fraction of the lubricant in the gaseous state continued to increase.
3. As the pressure increased with change in temperature and rotational speed, the angle of the resultant force moved in a direction close to the minimum lubricating thickness, and this change increased as the eccentricity increased.
4. By introducing the dimple structure, direct contact between the shaft and the bearing that occurs during solid lubrication is reduced. By changing the parameters of the dimple, the pressure on the bearing can be reduced while keeping the resultant force constant.

5. Due to the dimple structure, the rise in the lubricant temperature is reduced and the volume fraction reduction prevents erosion inside the bearing due to cavitation.



5. References

1. Tauviquirrahman, M., J. Jamari, and A.P. Bayuseno. *A comparative study of finite journal bearing in laminar and turbulent regimes using CFD (computational fluid dynamic)*. in *MATEC web of conferences*. 2016. EDP Sciences.
2. Aksoy, S. and M.F. Aksit, *A fully coupled 3D thermo-elastohydrodynamics model for a bump-type compliant foil journal bearing*. Tribology International, 2015. **82**: p. 110-122.
3. Farrall, M., et al. *A numerical model for oil film flow in an aero-engine bearing chamber and comparison with experimental data*. in *Turbo Expo: Power for Land, Sea, and Air*. 2004.
4. Raimondi, A. and J. Boyd, *A solution for the finite journal bearing and its application to analysis and design: III*. ASLE Transactions, 1958. **1**(1): p. 194-209.
5. Dai, F. and M. Khonsari, *A theory of hydrodynamic lubrication involving the mixture of two fluids*. 1994.
6. Andrade, E.d.C., *XLI. A theory of the viscosity of liquids.—Part I*. The London, Edinburgh, and Dublin Philosophical Magazine and Journal of Science, 1934. **17**(112): p. 497-511.
7. Dhande, D. and D. Pande, *A two-way FSI analysis of multiphase flow in hydrodynamic journal bearing with cavitation*. Journal of the Brazilian

Society of Mechanical Sciences and Engineering, 2017. **39**(9): p. 3399-3412.

8. Armentrout, R.W., et al., *Analysis of turbulence and convective inertia in a water-lubricated tilting-pad journal bearing using conventional and cfd approaches*. Tribology Transactions, 2017. **60**(6): p. 1129-1147.
9. Lin, Q., et al., *Analysis on the lubrication performances of journal bearing system using computational fluid dynamics and fluid–structure interaction considering thermal influence and cavitation*. Tribology international, 2013. **64**: p. 8-15.
10. Guo, Z., T. Hirano, and R.G. Kirk, *Application of CFD analysis for rotating machinery—Part I: hydrodynamic, hydrostatic bearings and squeeze film damper*. J. Eng. Gas Turbines Power, 2005. **127**(2): p. 445-451.
11. Constantinescu, V., *Basic relationships in turbulent lubrication and their extension to include thermal effects*. 1973.
12. Jourak, A., *CFD Analysis of a Journal Bearing with a Microgroove on the Shaft*. 2008.
13. Gertzog, K., P. Nikolakopoulos, and C. Papadopoulos, *CFD analysis of journal bearing hydrodynamic lubrication by Bingham lubricant*. Tribology International, 2008. **41**(12): p. 1190-1204.

14. Gengyuan, G., et al., *CFD analysis of load-carrying capacity of hydrodynamic lubrication on a water-lubricated journal bearing*. Industrial Lubrication and Tribology, 2015.
15. Manshoor, B., et al., *CFD analysis of thin film lubricated journal bearing*. 2013.
16. Yong, H. and R. Balendra. *CFD analysis on the lubrication behaviours of journal bearing with dimples*. in *2009 International Conference on Mechatronics and Automation*. 2009. IEEE.
17. Uhkoetter, S., et al. *Development and validation of a three-dimensional multiphase flow CFD analysis for journal bearings in steam and heavy duty gas turbines*. in *Turbo Expo: Power for Land, Sea, and Air*. 2012. American Society of Mechanical Engineers.
18. Sun, J. and G. Changlin, *Hydrodynamic lubrication analysis of journal bearing considering misalignment caused by shaft deformation*. Tribology International, 2004. **37**(10): p. 841-848.
19. Jiang, N.J., Y.L. Peng, and F.L. Wu. *Improve Journal Bearing Design Using Numerical Method*. in *Applied Mechanics and Materials*. 2011. Trans Tech Publ.
20. Ermolaev, M., V. Batishchev, and K. Goryachev, *Investigation of the vapor pressure of lubricating oils*. Chemistry and Technology of Fuels and Oils, 1972. **8**(5): p. 388-390.

21. Reynolds, O., IV. *On the theory of lubrication and its application to Mr. Beauchamp tower's experiments, including an experimental determination of the viscosity of olive oil.* Philosophical transactions of the Royal Society of London, 1886(177): p. 157-234.
22. Fouflias, D.G., et al., *Performance comparison between textured, pocket, and tapered-land sector-pad thrust bearings using computational fluid dynamics thermohydrodynamic analysis.* Proceedings of the Institution of Mechanical Engineers, Part J: Journal of Engineering Tribology, 2015. **229**(4): p. 376-397.
23. Kvitnitsky, Y., N. Kirkatch, and Y. Poltavsky, *The solution of reynolds equation under natural boundary conditions for hydrodynamic journal bearings.* Wear, 1976. **37**(2): p. 217-231.
24. Orcutt, F. and E. Arwas, *The steady-state and dynamic characteristics of a full circular bearing and a partial arc bearing in the laminar and turbulent flow regimes.* 1967.
25. Sahu, M., A.K. Giri, and A. Das, *Thermohydrodynamic analysis of a journal bearing using CFD as a tool.* Int. J. Sci. Res. Publ, 2012. **2**(9): p. 1-7.
26. Singla, A., et al. *Thermo-hydrodynamic analysis on temperature profile of circular journal bearing using computational fluid dynamics.* in *2014 Recent Advances in Engineering and Computational Sciences (RAECS)*. 2014. IEEE.

27. Chun, S.M., *Thermohydrodynamic lubrication analysis of high-speed journal bearing considering variable density and variable specific heat*. Tribology International, 2004. **37**(5): p. 405-413.
28. Hanoca, P. and H. Ramakrishna, *To Investigate the Effect of Oil Film Thickness at the Entrance of the Infinitely Long Slider Bearing Using CFD Analysis*. Procedia Engineering, 2015. **127**: p. 447-454.
29. *KS B ISO7902-1 Plain bearings — Hydrodynamic plain journal bearings under steady-state conditions — Circular cylindrical bearings — Part 1: Calculation procedure*. 2016, Korean Industry Council: Korea.
30. Menter, F. and C. Rumsey. *Assessment of two-equation turbulence models for transonic flows*. in *Fluid Dynamics Conference*. 1994.
31. ANSYS, *Release 18.2, ANSYS CFX-Solver Modeling Guide*, ANSYS Inc, . 2018.
32. Dhande, D. and D. Pande, *Multiphase flow analysis of hydrodynamic journal bearing using CFD coupled fluid structure interaction considering cavitation*. Journal of King Saud University-Engineering Sciences, 2018. **30**(4): p. 345-354.
33. Hughes, W. and F. Osterle, *Temperature effects in journal bearing lubrication*. ASLE Transactions, 1958. **1**(1): p. 210-212.
34. Andrade, E.N.D.C., *On the viscous flow in metals, and allied phenomena*. Proceedings of the Royal Society of London. Series A,

Containing Papers of a Mathematical and Physical Character, 1910.
84(567): p. 1-12.

